



<https://theses.gla.ac.uk/>

Theses Digitisation:

<https://www.gla.ac.uk/myglasgow/research/enlighten/theses/digitisation/>

This is a digitised version of the original print thesis.

Copyright and moral rights for this work are retained by the author

A copy can be downloaded for personal non-commercial research or study,  
without prior permission or charge

This work cannot be reproduced or quoted extensively from without first  
obtaining permission in writing from the author

The content must not be changed in any way or sold commercially in any  
format or medium without the formal permission of the author

When referring to this work, full bibliographic details including the author,  
title, awarding institution and date of the thesis must be given

Enlighten: Theses

<https://theses.gla.ac.uk/>  
[research-enlighten@glasgow.ac.uk](mailto:research-enlighten@glasgow.ac.uk)

INITIAL OPERATION OF THE GLASGOW

300 MEV ELECTRON SYNCHROTRON

D. L. OLDROYD

THESIS

SUBMITTED TO THE

UNIVERSITY OF GLASGOW

FOR THE

DEGREE OF DOCTOR OF PHILOSOPHY

ProQuest Number: 10646764

All rights reserved

INFORMATION TO ALL USERS

The quality of this reproduction is dependent upon the quality of the copy submitted.

In the unlikely event that the author did not send a complete manuscript and there are missing pages, these will be noted. Also, if material had to be removed, a note will indicate the deletion.



ProQuest 10646764

Published by ProQuest LLC (2017). Copyright of the Dissertation is held by the Author.

All rights reserved.

This work is protected against unauthorized copying under Title 17, United States Code  
Microform Edition © ProQuest LLC.

ProQuest LLC.  
789 East Eisenhower Parkway  
P.O. Box 1346  
Ann Arbor, MI 48106 – 1346

## CONTENTS

### PREFACE

#### CHAPTER 1.

#### BASIC PRINCIPLES OF BETATRON AND SYNCHROTRON ACCELERATION 5

- 1.1 Introduction.
- 1.2 The Betatron.
- 1.3 Focusing Requirements of the Guide Field.
- 1.4 Synchrotron Acceleration.
- 1.5 Field Inhomogeneities.

#### CHAPTER 2.

#### THE GLASGOW 300 MEV ELECTRON SYNCHROTRON 21

- 2.1 Introduction.
- 2.2 Magnet Assembly.
- 2.3 Excitation System.
- 2.4 Vacuum System.
- 2.5 Electronic Equipment.
- 2.6 Control.

#### CHAPTER 3.

#### THE SEARCH FOR A BEAM 51

- 3.1 General Approach to the Problem.
- 3.2 Scintillation Probes.
- 3.3 Use of the Probes to find a Betatron Beam.
- 3.4 Synchrotron Operation.
- 3.5 Intensity Measurements.

#### CHAPTER 4.

#### RF SHAPING EXPERIMENTS 96

- 4.1 Introduction.
- 4.2 RF Front Edge Shaping.
- 4.3 Experimental Results.

#### CHAPTER 5.

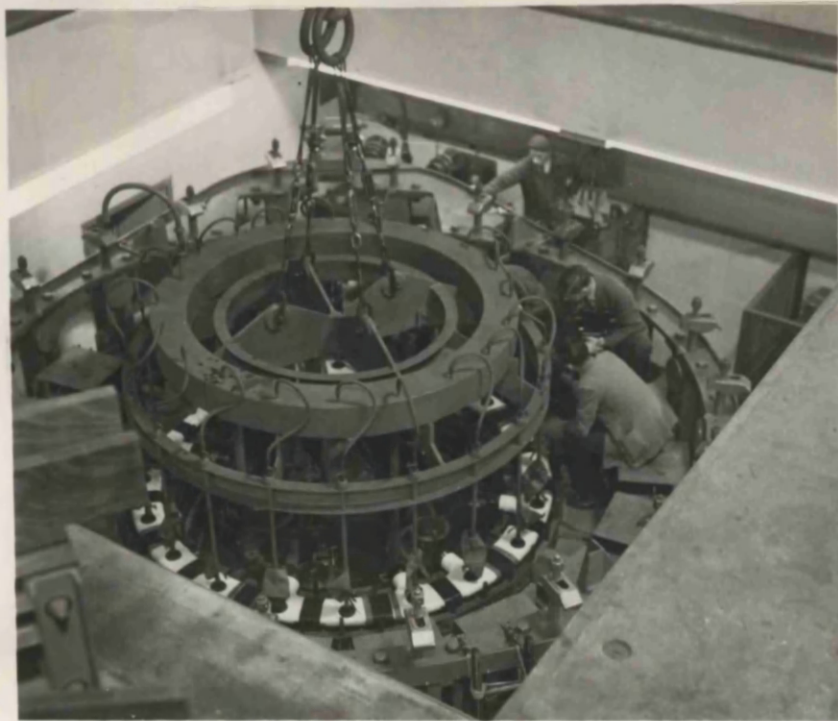
#### MISCELLANEOUS EXPERIMENTS 111

- 5.1 Betatron Output Variation with Gun Parameters.
- 5.2 Aperture Experiments.

#### CHAPTER 6.

#### USE OF THE SYNCHROTRON IN NUCLEAR PHYSICS 119

#### REFERENCES 125



DONUT INSTALLATION

*The entire donut is evacuated and then lowered into position as one unit.*



## PREFACE

This thesis consists mainly of an account of the work carried out to render operational the 300 MeV synchrotron at Glasgow University from the time at which installation and general testing were completed.

Detailed descriptions are given of the particular contributions made by the author, who was associated with the project during the period 1949 - 1954 whilst working for the Ph.D. degree.

The first chapter is a preliminary summary of the principles underlying the acceleration of electrons to high energies in the betatron and synchrotron.

A brief account, in chapter two, of the Glasgow installation serves to illustrate the practical realization of these principles, and brings out the salient operational features of the machine.

Chapter three is an account of the methods and technique employed in the establishment of the X-ray beam. The development of sensitive detectors embodying the principles of the scintillation counter, and the subsequent successful employment of these in the initial search for a beam are reported in detail.

In chapters four and five, various experiments carried out on the internal electron beam and external X-ray beam are described.

A note on the use of the synchrotron in nuclear physics concludes the thesis.

Original work by the author includes the modifications to the electronic gear described in chapter two; the development of the scintillation probes, chapter three; the shaping experiments on the RF waveform, chapter four; and the beam experiments of chapter five.

The actual search for the beam and the execution of the beam experiments were carried out in collaboration with Dr. W. McFarlane and Mr. S. E. Barden, the other members of the synchrotron research team.

The author wishes to express his gratitude to these two colleagues and also to Professor P. I. Dee for sustained interest and encouragement.

D. L. Oldroyd

November 1954

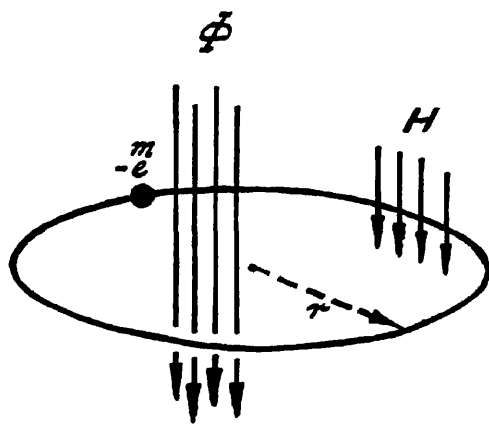


FIG. 1

---

## CHAPTER 1

### PRINCIPLES OF BETATRON AND SYNCHROTRON ACCELERATION

#### 1.1 Introduction.

In the electron synchrotron, acceleration proceeds in two stages. Electrons injected at 50-100 keV are accelerated by betatron action to an energy of 2-5 MeV and then by synchrotron action to the final energy.

This arrangement is constructionally advantageous since the whole acceleration occurs in circular orbits of sensibly constant radius.

The papers of Kerst and Serber 1, 2, 3, and of Bohm and Foldy 4 form the basis of the following summary.

#### 1.2 The Betatron.

The magnetic field in a betatron consists of two parts: a radially symmetrical guide field,  $H$ , which constrains the electrons to plane circular orbits perpendicular to itself, and a central orbit-linking field. Fig. 1.

The radius,  $r$ , of the orbit, or instantaneous circle, is given (in Gaussian units) by

$$\frac{eH}{c} = \frac{p}{r} \quad (1)$$

$e$  being the charge and  $p$  the momentum of a particle.  $c$  is the velocity of light in vacuo.

If the central flux  $\oint$  linking the orbit is increased, the electrons are accelerated by the induced electric field

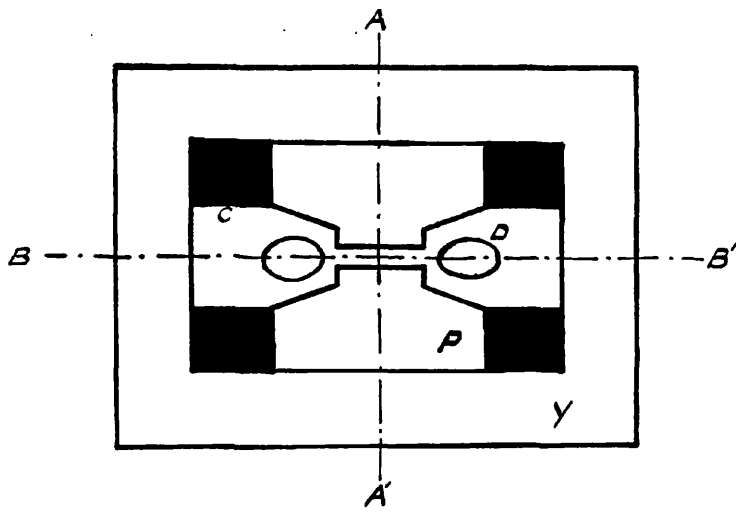


FIG. 2

---

and tend to move to a larger orbit. However, if the guide field increases in direct proportion to the momentum, acceleration proceeds in the same orbit. This obtains if the rates of change of guide field and accelerating flux are proportional: specifically

$$\frac{\partial H}{\partial t} = \frac{1}{2\pi r_0^2} \frac{\partial \Phi}{\partial t} \quad (2)$$

where  $r_0$  is the radius of the betatron orbit.

Fig. 2 represents a vertical section of a betatron electromagnet - a laminated steel structure comprising circular polepieces P, yoke Y, and excitation coils C mounted round the poles. This produces a field radially symmetrical about the vertical centre line AA' and everywhere normal to the median plane BB'. The strong orbit-linking field occurs across the narrow central gap and the weaker guide field at D where the non-magnetic toroidal vacuum chamber, or donut, is situated. The central gap is adjusted so that the betatron orbit is at the centre of the donut.

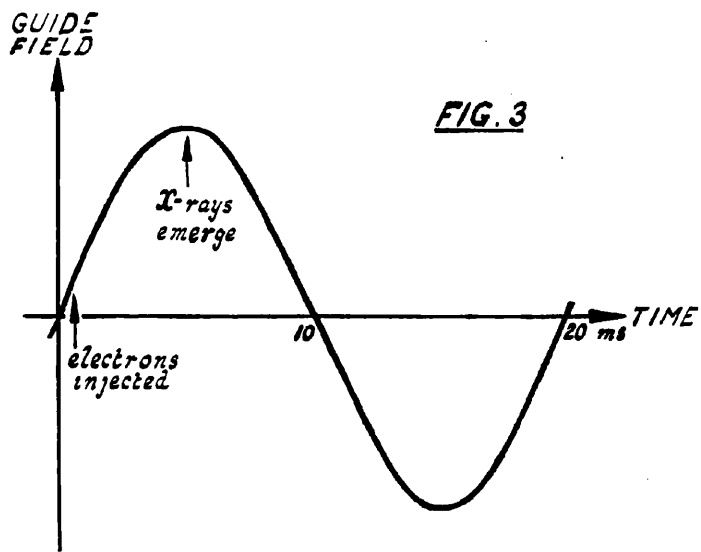
An electron in the orbit has total energy W given in electron-volts by

$$W^2 = 9 \times 10^4 H^2 r^2 + W_m^2 \quad (3)$$

where  $W_m$  is the rest energy. For  $W > 10$  MeV,  $W^2 \gg W_m^2$  and (3) reduces to

$$W = 300 H r \quad (4)$$

From (3) it follows that for a given orbit radius, a one-to-one correspondence exists between guide field



strength  $H$  and particle energy  $W$ .

The magnet is excited sinusoidally (usually at fifty cycles per second) and the electrons are injected tangentially into the donut from a low energy gun at guide field strengths near zero. During the next quarter cycle of field variation, acceleration proceeds but as peak field is approached the central core saturates, so that  $\frac{\partial \phi}{\partial t}$  does not keep in step with  $\frac{\partial H}{\partial t}$  and the electrons spiral inwards. They hit the back of the gun and produce X-rays which emerge from the machine in a narrow beam.

The donut is continuously evacuated to reduce loss of electrons by collision with gas molecules.

Fig. 3 indicates the operational cycle.

### 1.3 Focusing Requirements of the Guide Field.

The orbits given by (1) must be stable, since the electrons may be displaced by collision with residual gas atoms or by mutual interaction. Further, the use of an internal gun precludes direct injection into the betatron orbit  $r_0$ , since the gun structure would obstruct particles after one revolution. Thus the injection radius  $r_{inj} \neq r_0$  and the particles must be focused on to the betatron orbit during acceleration.

By weakening the field with increasing radius, so that

$$H \propto \frac{1}{r^n} \quad , \quad 0 < n < 1 \quad (5)$$

these requirements are met.

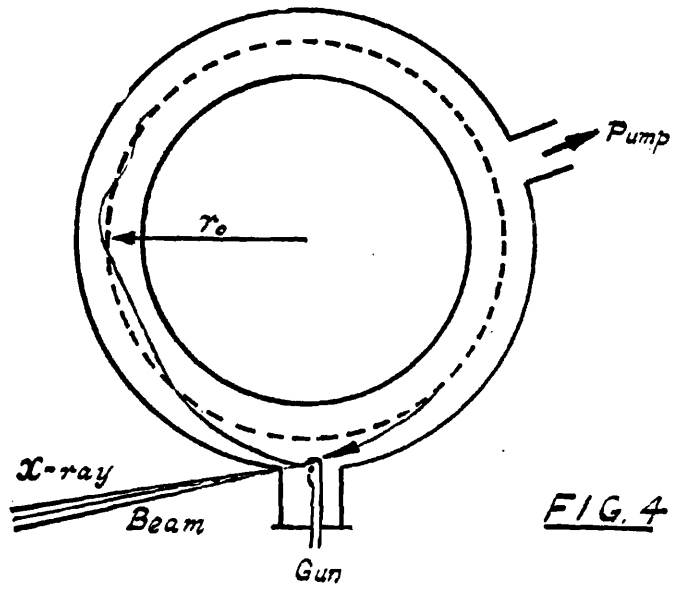


FIG. 4

Particles displaced from their instantaneous circles, as given by (1), execute stable free oscillations about them with frequencies  $f_p \sqrt{1-n}$  radially,  $f_p \sqrt{n}$  axially: where  $f_p$  is the frequency of revolution of the electron. Furthermore, particles are focused into the median plane.

As the field increases, the instantaneous circles expand or contract to the betatron orbit, while the amplitude of the free oscillations diminishes.

At injection, the instantaneous circle is

$$r_i = \frac{c p_{inj}}{e H_{inj}} \quad (6)$$

In practice, injection with a sensibly constant  $p_{inj}$  occurs over a short finite time during which  $H_{inj}$  is increasing, with consequent decreasing  $r_i$ . Thus most electrons enter the donut undergoing oscillations with initial amplitude  $|r_i - r_{inj}|$ . Some of these will be too large and such electrons will hit the donut walls; some electrons will be trapped into stable orbits and damp down sufficiently to miss the gun on subsequent revolutions; a few will not oscillate, being injected at the instant when  $r_i = r_{inj}$ . As the field increases, all will eventually move on to the betatron orbit  $r_0$ , given by (2), lying in the median plane of the magnet.

Fig. 4 depicts a typical donut assembly - this is a glass or ceramic structure and the gun is introritted through a vacuum seal on the end of a port, the pumps being attached to other ports.

In fig. 4, electrons are injected at  $r_{inj} > r_0$ . The major part of the acceleration occurs at  $r_0$ , and when the magnet core saturates the electrons hit the gun and produce X-rays.

Electrons not trapped into stable orbits at injection, or later lost through scattering by residual gas atoms, would charge up the donut walls and disturb the trapped beam. In order to prevent this, the donut walls are metallized and this conducting coating is earthed.

Field disturbing eddy currents set up in the coating by the changing magnetic field are kept to a minimum by appropriate scribing and by confining the coating thickness to a few skin depths.

The upper energy limit achievable is set by radiation losses which are proportional to the fourth power of the electron energy; when this balances the energy gained by induction the limit is reached. For a machine of practicable size this ceiling is estimated at 500 MeV, 5-10.

Details of specific machines and developments of the betatron are given in the extensive literature, 11-37.

#### 1.4 Synchrotron Acceleration.

In the synchrotron, electrons are confined to an annular region by a magnetic field identical to a betatron guide field. The magnet has no central region however, the acceleration being produced by an alternating electric field generated tangentially at some point in the orbit.

This is usually achieved by constructing part of the donut in the form of a quarter-wave coaxial resonator and arranging that the voltage antinode occurs across a narrow gap in the inner coating (fig. 19).

The resonator is energized by an RF oscillator at angular frequency  $\omega_{AC}$  equal to the angular velocity of a photon in the annulus mean orbit.

The gap voltage is sinusoidal

$$v_{gap} = V \sin(\omega_{AC} t) \quad (7)$$

From (1) the angular velocity of the electron

$$\omega_p = \frac{v}{r} = \frac{e c H}{W} \quad (8)$$

where  $v$ ,  $W$  are the velocity and total energy respectively.

$$W = \frac{m c^2}{\sqrt{1 - \frac{v^2}{c^2}}} \quad (9)$$

$m$  being the electron mass.

In a constant guide field  $H$ , an electron revolving with  $\omega_p = \omega_{AC}$  would always be in step with the resonator voltage if it first crossed the gap at a zero voltage instant. It would experience no change in its synchronous energy  $W_s$ : from (8)

$$W_s = \frac{e c H}{\omega_{AC}} \quad (10)$$

(10) with (9) gives the synchronous velocity  $v_s$  and then the synchronous radius  $r_s$  is

$$r_s = \frac{v_s}{\omega_{AC}} \quad (11)$$

An electron which crosses the gap when the voltage is not zero undergoes an energy change  $e v_{gap}$ . From (8), (9) it is seen that a change of energy is accompanied by

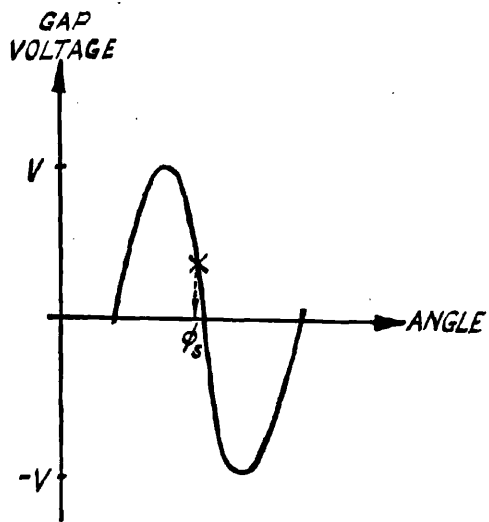
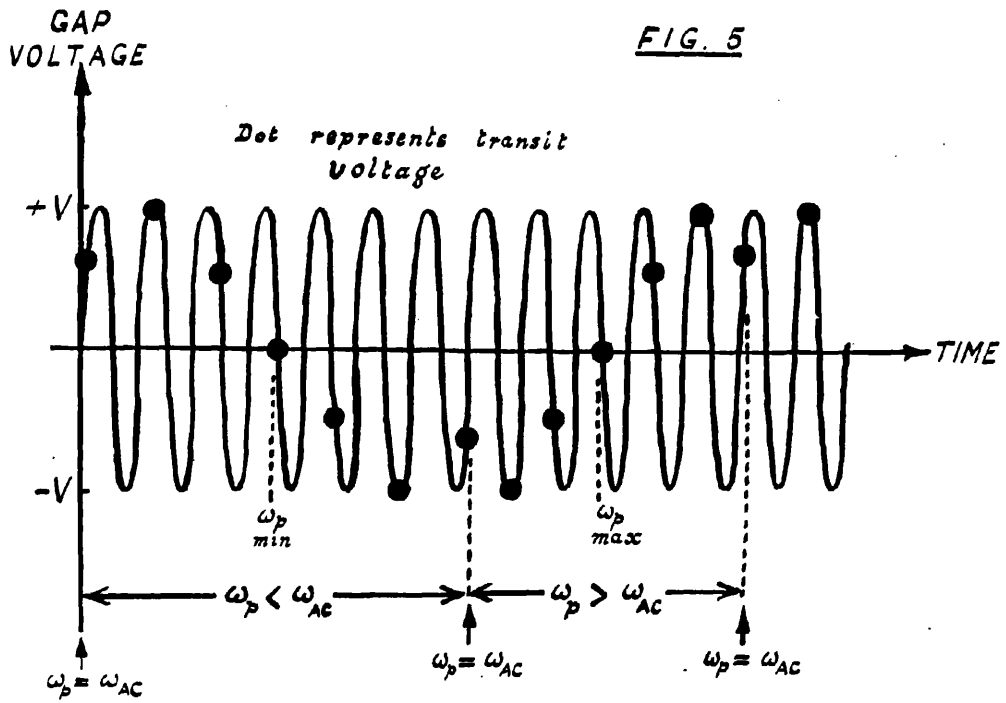


FIG. 6

changes of velocity and radius of the same sign, and a change of angular velocity of opposite sign, so that the electron next crosses the gap at a slightly different value of gap voltage.

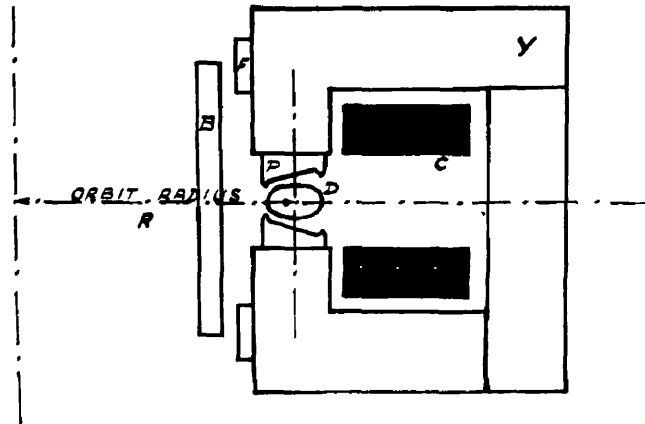
The overall effects of successive transits are that the energy, radius, and angular velocity of the electron undergo oscillations about the synchronous values  $W_s$ ,  $r_s$ ,  $\omega_{AC}$ . So long as  $H$  and  $\omega_{AC}$  are constant the particle suffers no permanent change in energy.

Fig. 5 illustrates one cycle of phase oscillation of gap transit; the stable, synchronous phase, for fixed  $H$ , is the zero point when the gap voltage is passing from positive to negative.

In practice the phase oscillation is considerably slower than fig. 5 suggests.

The stability of these oscillations depends on the amplitude of the gap voltage and on the initial transit phase.

A small increase in the guide field, from  $H$  to  $H'$ , shifts the synchronous energy to  $W'_s = \frac{ecH'}{\omega_{AC}} > W_s$ . The particle motion now changes so that the energy oscillates about the new value  $W'_s$ . If the guide field increases continuously at a slow rate, such that the change in field is small in one period of phase oscillation, the particle energy increases with  $H$ . The synchronous phase now moves back from the zero point to a value  $\phi_s$  (fig. 6) such that a



C : EXCITATION COILS  
 Y : YOKE  
 P : POLEPIECE  
 B : FLUX BAR  
 F : FLUX PAD  
 D : DONUT

FIG. 7

synchronous electron gains sufficient energy  $eV\sin\phi_s$ , on each transit, to move out with the synchronous orbit. Phase oscillations of non-synchronous electrons now take place about  $\phi_s$ .

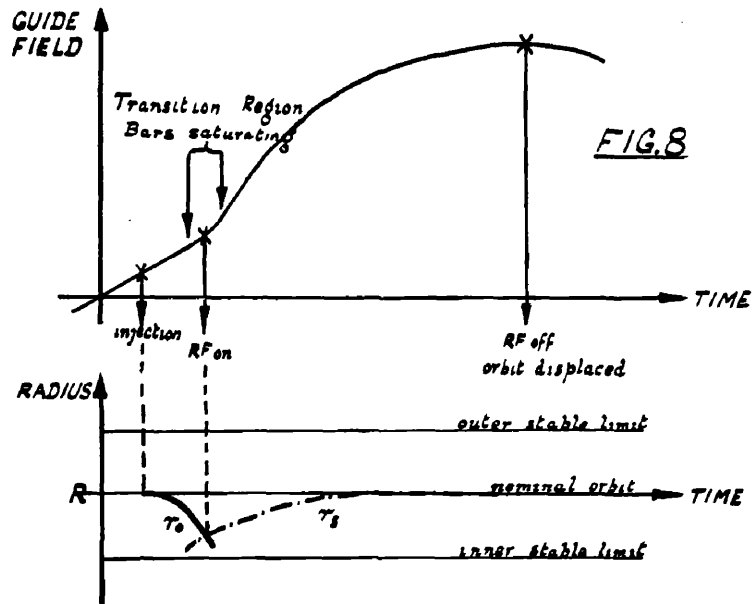
Bohm and Foldy 4 give quantitative expressions for synchrotron motion, and show that, as the guide field increases, the phase oscillations are damped out. Thus the synchronous orbit is the one on which particles finally move.

The advantage of betatron starting now emerges. From (11) it is seen that  $r_s \propto v_s$  and  $\frac{v_s}{c} \rightarrow 1$  as the energy increases. For electrons of energy 2 MeV,  $\frac{v}{c} = 0.98$  so that only a 2% variation of  $r_s$  occurs above 2 MeV, as  $\frac{v}{c} \rightarrow 1$ . By constructing the magnet to act initially as a betatron, such that the betatron and limiting synchronous orbits coincide, the guide field can be kept to a narrow annulus and a smooth transition made from betatron to synchrotron action.

Instead of a large central core, the magnet has several flux bars which saturate when the electron energy reaches  $\sim 2$  MeV. Fig. 7 illustrates a typical arrangement.

The electrons are injected into the donut from a hot-filament electron gun at 50-100 keV and accelerated at the nominal orbit radius  $R$  by betatron action. As the energy approaches  $\sim 2$  MeV the flux bars begin to saturate and the betatron orbit decreases. At some instant it is equal to the synchronous orbit and the resonator is energized near





this time. The electrons then experience phase bunching - some with too large initial phase oscillations will be lost - and are carried to peak energy by synchrotron action. At peak field the RF is switched off and the electron beam is displaced on to a target to produce X-rays.

Fig. 8 shows the operational sequence and the variation of the stable orbit radius during acceleration. The horizontal lines indicate the limits of the stable region of the guide field within which  $0 < n < 1$ . The transition radius must be inside these limits (and inside the donut) to allow successful changeover.

The magnet is excited sinusoidally but the field is not sinusoidal owing to the presence of the saturable flux bars.

Higher energies are attainable than in the betatron since the resonator power offsets radiation losses; a machine of 1500 MeV energy is under construction.

Details of particular installations and specific topics are given in the literature 38-57.

### 1.5 Field Inhomogeneities.

The guide field is designed to have azimuthal homogeneity and axial symmetry about the median plane. In addition, for stable orbits, there is a radial dependence given by (5).

Variations in quality of materials and assembly,

together with localized hysteresis and eddy current effects, give rise to out-of-phase fields which result in azimuthal inhomogeneities (these distort the electron orbits) and axial asymmetries (these modify the effective n-value).

Both effects are especially serious at injection when the field is low, and large inhomogeneities may give rise to unstable orbit conditions with consequent partial or total loss of injected electrons.

To counteract such irregularities, suitably driven field correction coils are incorporated at appropriate places in the magnet.

## CHAPTER 2

### THE GLASGOW 300 MEV ELECTRON SYNCHROTRON

#### 2.1 Introduction.

The Glasgow machine was designed to operate initially at 300 MeV with nominal orbit radius 125 cm at a guide field strength 8000 oe.

Injection voltages up to 100 kV can be used and transition from betatron to synchrotron action occurs at ~5 MeV.

To produce X-rays, the internal electron beam is either expanded on to an external target or allowed to contract, after peak field, on to an internal one.

The guide field index  $n$  is 0.7 and the RF oscillator frequency is 38.2 Mc/s.

Excitation of the magnet occurs five times per second and the acceleration time is six milliseconds.

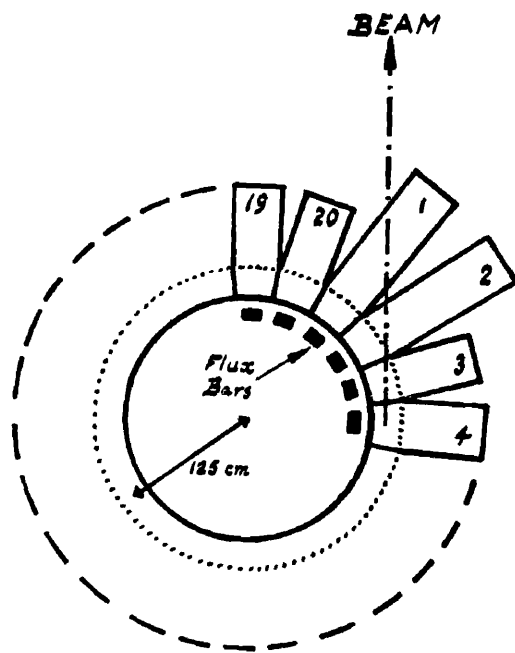
In the following sections the component parts of the synchrotron assembly are briefly discussed.

#### 2.2 Magnet Assembly.

##### 2.2.1 General.

The magnet comprises twenty rectangular cee sections, as in fig. 7, evenly distributed round a circle with the pole-piece wedges butting together to form a continuous circle for the guide field. Vertical steel laminations of





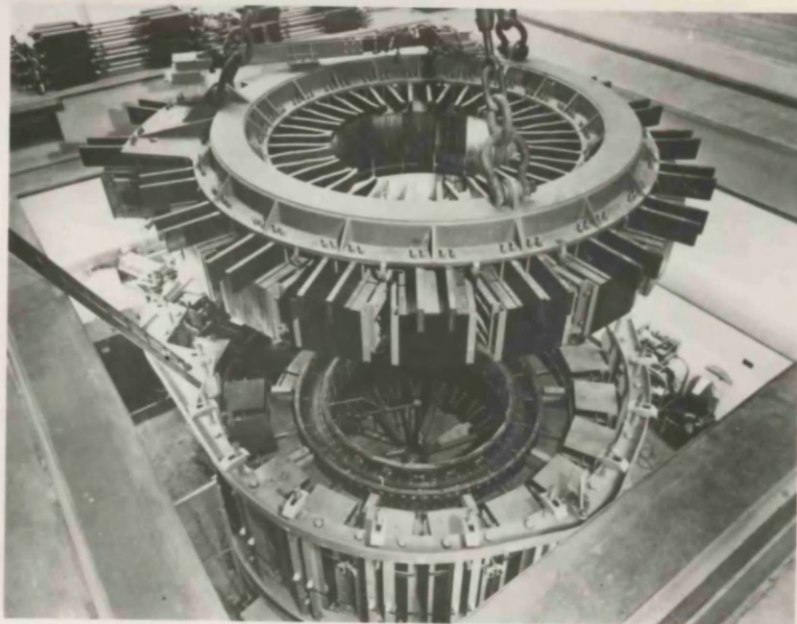
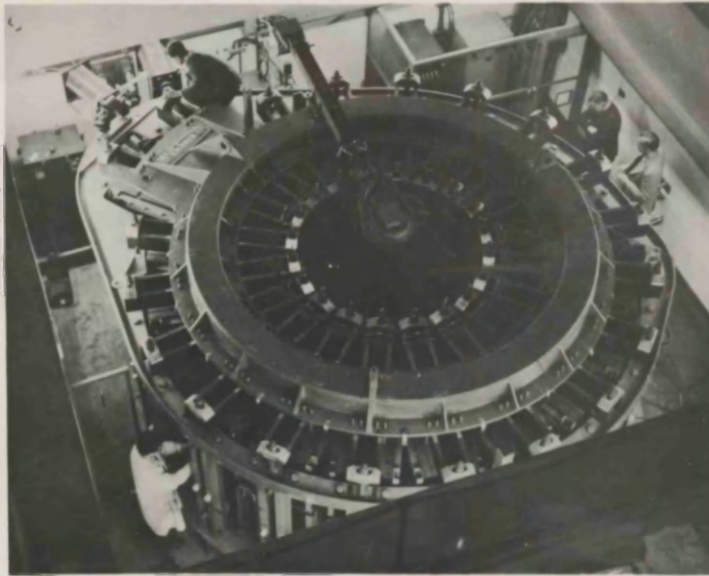
CEE ARRANGEMENT  
GLASGOW SYNCHROTRON

FIG. 9





Fig. 10



0.014 in are used in the yoke sections and 0.007 in for the flux bars. Transversely laminated pads carry the flux from yoke to bars. Two cees are elongated horizontally to provide a window for the emerging X-rays (fig. 9).

The excitation coils consist of twenty turns in identical upper and lower sections of ten turns each, encircling the poles inside the cees; at 300 MeV these carry a peak current of 3300 amperes.

Each cee is in three sections, and in order to gain access to the donut, all twenty top limbs, top pole-pieces and upper set of coils can be lifted out as one fortyone ton unit. (Fig. 10).

A field index  $n = 0.7$  is obtained from a  $1.5^\circ$  taper on each poleface; the gap size is approximately 7 in radially by 4 in axially.

Poleface edge lips correct fringing.

The magnet weighs 120 tons of which 75 tons are active steel. It sits on sixty double elliptical springs over a pit which houses the vacuum equipment. Cooling air is blown up from the pit.

Fig. 10 shows the magnet which is situated below ground level in a thick-walled concrete chamber, the roof of which slides into a recess to give access for manipulation.

### 2.2.2 Correction Coils.

Twenty coils, each wound round one flux bar, are

connected in parallel across a motor-controlled variable reactor; this arrangement provides easy control of the position of the betatron orbit and ensures azimuthal uniformity of bar flux.

The out-of-phase fields caused by eddy currents and remanence in the yoke, which produce azimuthal field inhomogeneities, are corrected by means of coils wound round each back limb. Connected across these are variable resistors, with, in parallel, other variable resistors ganged in four sets corresponding to five adjacent cees per set. Thus corrections can be made over individual cees and over quadrantal sectors of the magnet, by means of the quadrature fluxes set up by the currents in the corrector coils.

Owing to the longer iron path, the guide field at the two extended cees is slightly weaker than elsewhere and produces an azimuthal first harmonic distortion in the field distribution. A single-turn coil enclosing the other eighteen back limbs is connected in series with a variable resistor and bucked against coils wound round the extended cees. In this way the extended cees are flux-forced by the others.

Variations in  $n$ , due to radial field inhomogeneities, are counteracted by single-turn, circular, poleface coils concentric with the orbit. These are balanced against a single-turn loop enclosing the total pole and bar flux, as



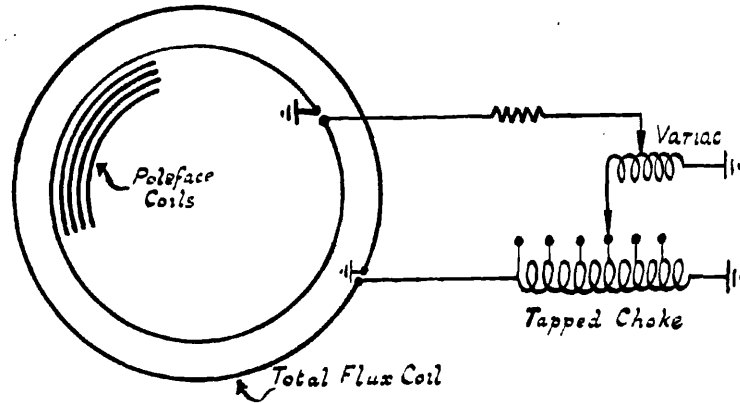


FIG. 11

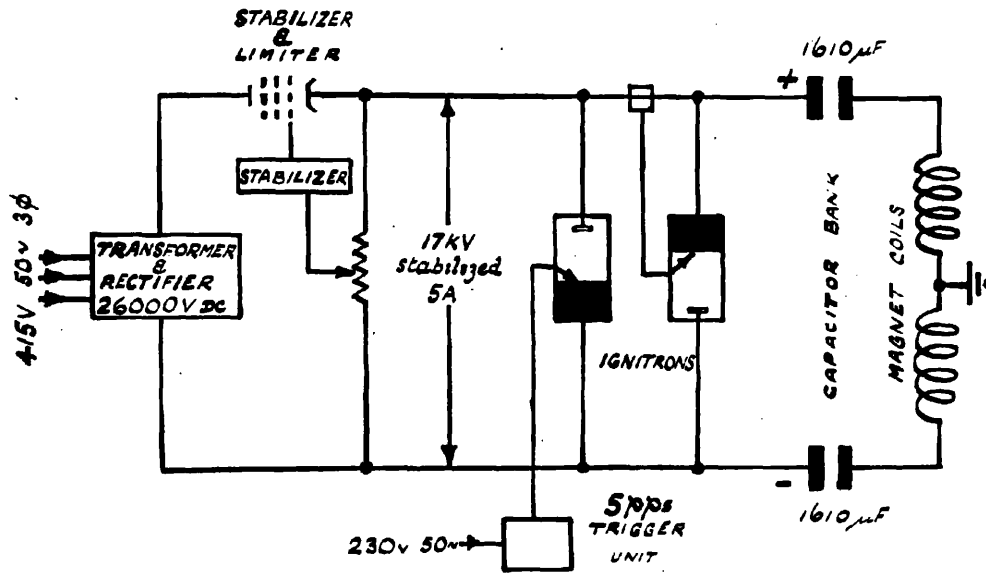


FIG. 12

in fig. 11, so that the correction current can be varied in either direction. Five such coils and driving loop are fitted on each poleface.

### 2.3 Excitation System.

The magnet is excited periodically by discharging a bank of capacitors into the coils. Fig. 12 is a block schematic of the excitation system.

A three-phase full-wave rectifier employs six CAR4 diodes to produce 26,000 V DC, stabilized to 17,000 V by a series pentode (type E1807) which also limits the output current to five amperes.

The 17 kV is applied to the capacitor bank which charges up through the coils, each leg taking 8.5 kV. Two back-to-back sets of four BK56 mercury pool pentode ignitrons in parallel discharge the capacitors into the coils. The leading ignitrons are fired from a mains-operated trigger unit, the trailing ones from a peaking current transformer on the busbar. A bias winding on this transformer gives control of the instant of commutation of the two sets of ignitrons.

This arrangement lets the coil-capacitor system oscillate for one cycle at sensibly the resonant frequency since the losses are small.

During the betatron period the magnet inductance is approximately 120 mH so that the resonant frequency is about 16 c/s; when the flux bars saturate the inductance decreases



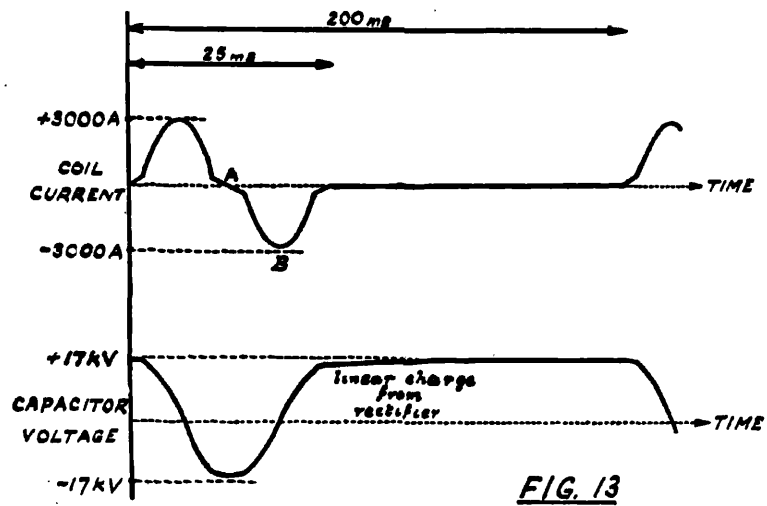


**FIG. 13**



FIG. 14

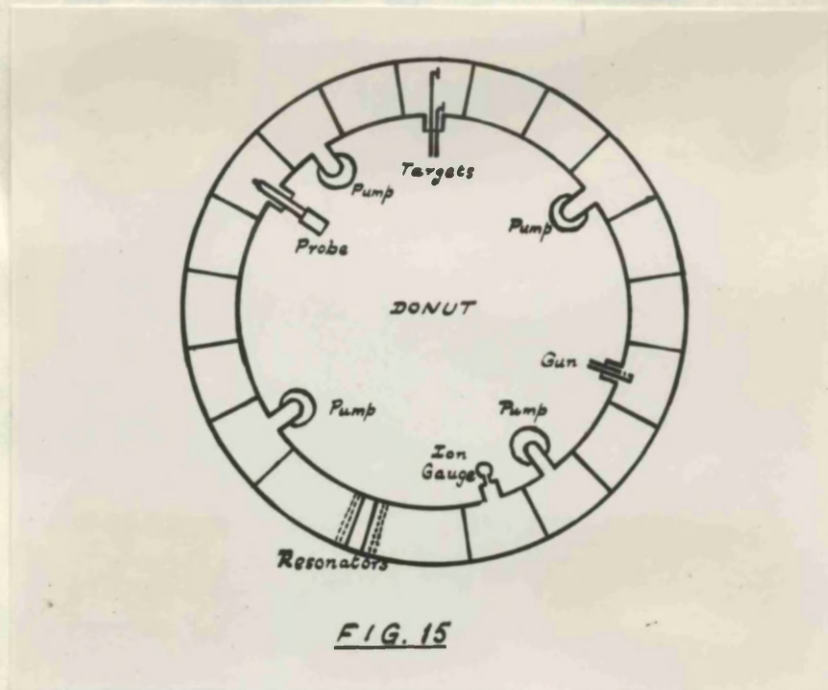


BK56 IGNITRONS



CAPACITORS





*BN 56 IONITRON*



Fig. 15b

to 20 mH and the frequency rises to 40 c/s. The current waveform is thus as in fig. 13; reaching a peak value of 3300 amps. with 805  $\mu$ F in circuit. This produces a peak guide field of 8000 oe. Also in fig. 13 is the capacitor voltage waveform, showing the rectifier making good the circuit losses between pulses .

Views of the ignitrons and capacitor bank are shown in fig. 14.

The capacitors are oil-immersed units of 115  $\mu$ F each: each leg has a total of 14 units for 300 MeV operation. Further units will be added to provide the larger peak currents required for higher operating energies; this procedure decreases the magnet frequency.

The normal operating recurrence frequency is five per second. Electrons are accelerated in the third quarter cycle i.e, AB of fig. 13.

A full account of the ignitrons is given in reference 58.

#### 2.4 Vacuum System.

The layout of the donut is sketched in fig. 15a; (a betatron donut is shown in fig. 15b). It comprises twenty pieces: plain sectors, port sectors, and resonators, separated by teflon gaskets and jointed with neoprene sleeves. All parts are of glazed porcelain called "frequentite" except the resonators which are of "tempradex" and unglazed.



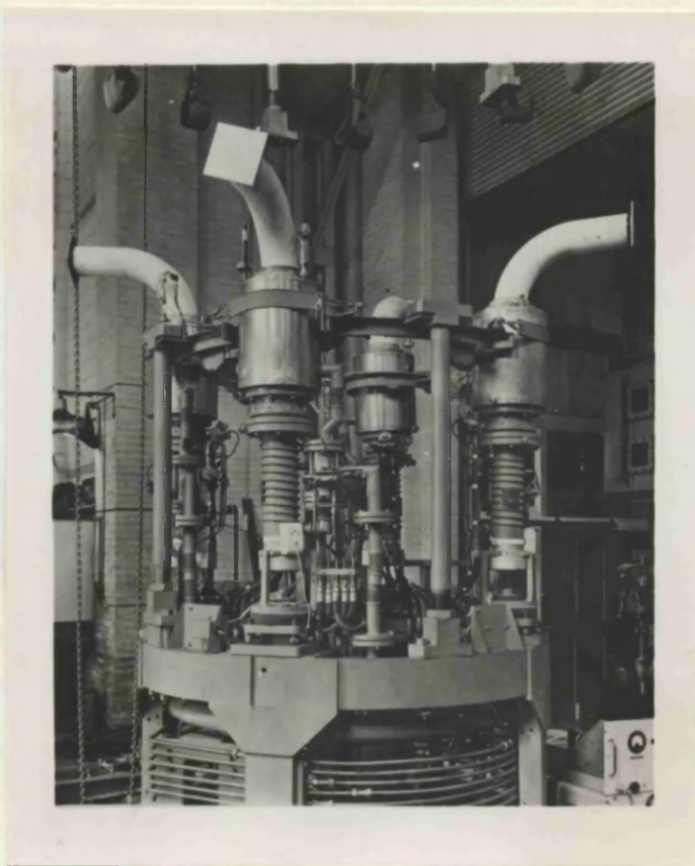
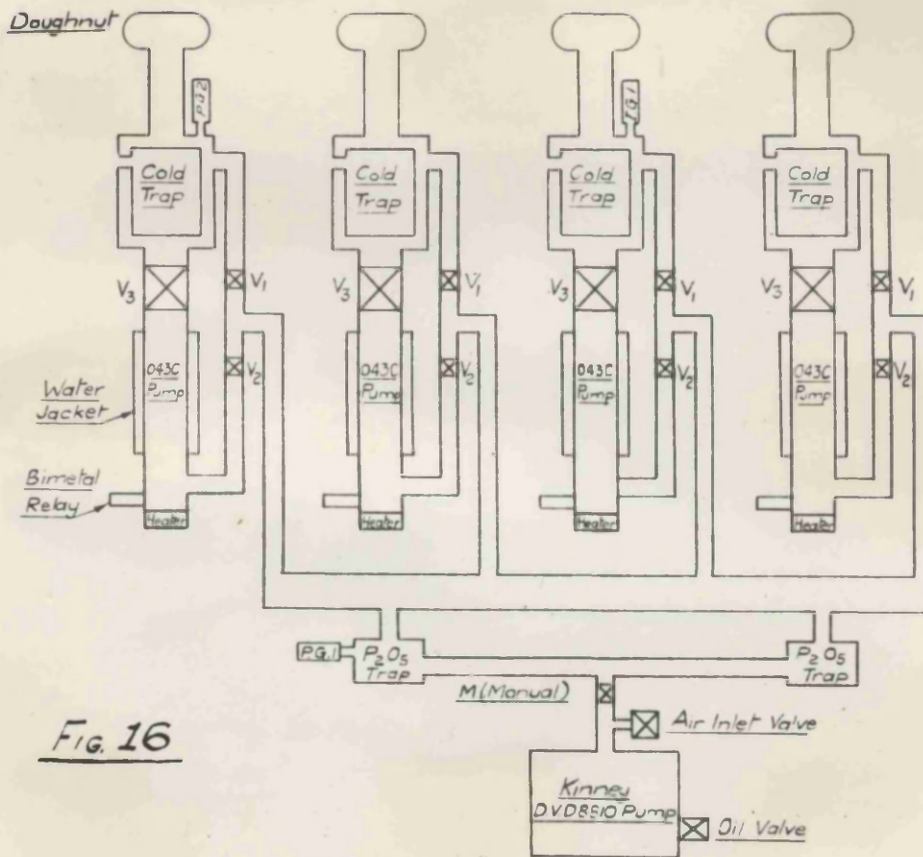


Fig. 17



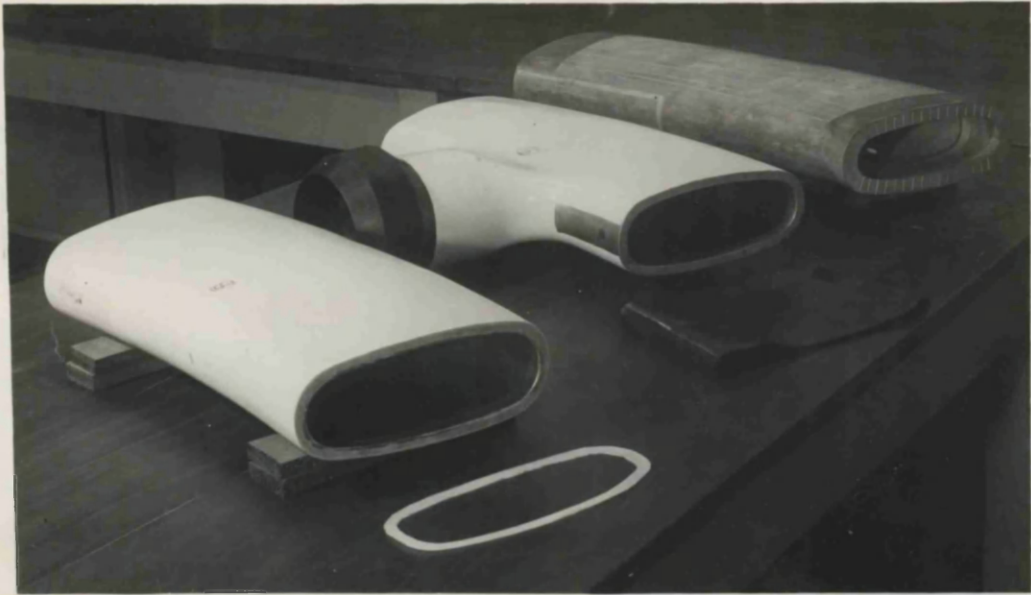


Fig. 18

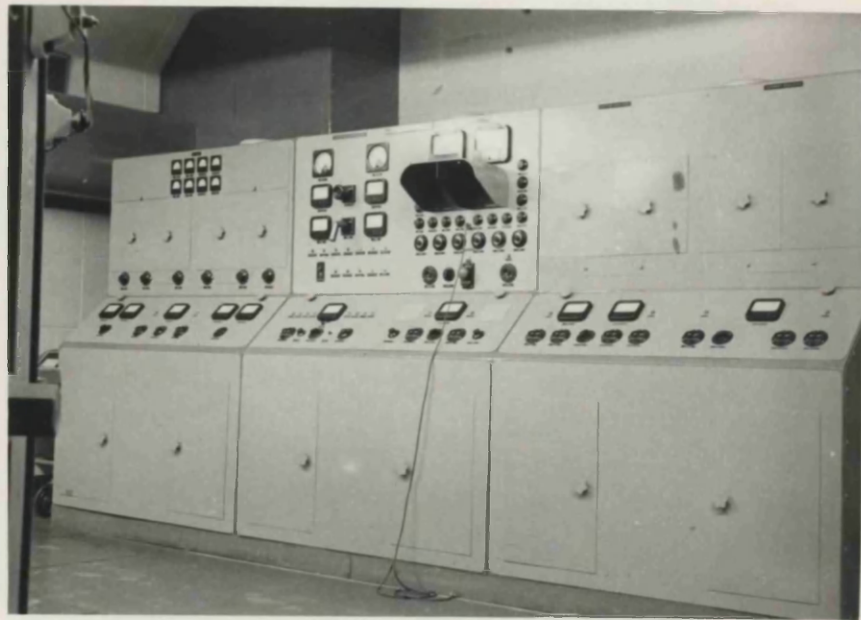


FIG. 54

The inside surfaces and the ends are platinized (resonators silvered) and these coatings are earthed through suitable resistors.

The pumping plant consists of four 4" oil diffusion pumps backed by a Kinney rotary pump, as in fig. 16, and the operating sequence is automatically controlled by two Pirani gauges. A compressed air system operates the valves. With liquid air in the cold traps, a donut pressure of  $10^{-6}$  mm Hg is quickly reached. An ionization gauge on the donut is interlocked with the injector gun and RF oscillator supplies and trips these if the donut pressure exceeds  $10^{-5}$  mm Hg.

Fig. 17 is a general view of the plant, while fig. 18 shows sectors, resonator, gasket and sleeve.

### 2.5 Electronic Equipment.

The equipment discussed briefly in this section, comprising the RF transmitter, the gun and orbit modulators, and the timing equipment, was built by A.E.R.E., Harwell, at T.R.E., Malvern, where the author spent a year assisting in its construction and testing.

After installation at Glasgow, subsequent modifications were called for as experience was gained in commissioning the synchrotron - these are indicated.

Fig. 54 shows the unit which is situated in the magnet chamber.



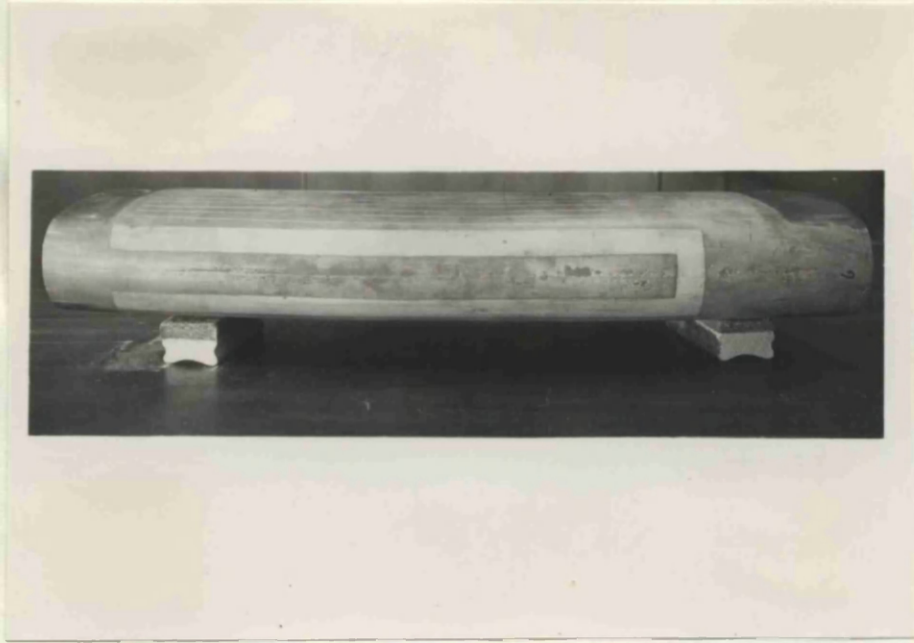


FIG 19



### 2.5.1 RF Equipment.

The RF oscillator provides power at 38.2 Mc/s to excite the two resonators. These are quarter-wave coaxial cavities constructed of  $\frac{1}{2}$  in thick tempradex to form part of the donut. A silver coating is fired on to the surface except at the accelerating gap and tongues, fig. 19.

To reduce eddy currents, the coating is scribed into laminations. The length of the resonator is  $\frac{\lambda}{4} \epsilon^{\frac{1}{2}}$ ;  $\lambda$  being the free-space wavelength of a 38.2 Mc/s wave and  $\epsilon$  the permittivity of the porcelain.

The feed from the oscillator is attached at a matching tongue on the inner edge, while a copper shorting strap across another tongue on the outer edge tunes the resonator.

An electron in the synchronous orbit has an energy gain per revolution

$$W_t = \frac{2\pi}{\omega_{AC}} \dot{W}_s \quad (\text{erg}) \quad (12)$$

$$= \frac{2\pi r_s}{c} \hat{W}_s \Omega_s \cos(\Omega_s t) \quad (\text{eV}) \quad (13)$$

using the relations:

$$\dot{W}_s = \frac{e c H_s}{\omega_{AC}} \quad (10)$$

$$\omega_{AC} = \frac{c}{r_s} \quad (14)$$

$$\hat{W}_s = 300 \hat{H}_s r_s \quad (4)$$

and setting

$$H_s = \hat{H}_s \sin(\Omega_s t) \quad (15)$$

The circumflex indicates peak value.

Thus 
$$(W_t)_{max} = \frac{2\pi r_s}{c} \hat{W}_s \Omega_s \quad (\text{eV}) \quad (16)$$

As the synchrotron phase commences some 100 $\mu$ s after field



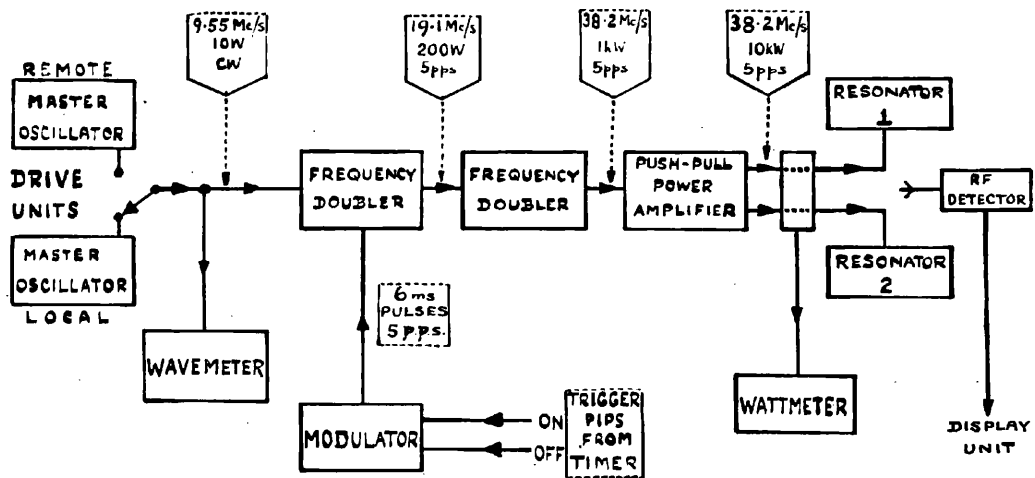


FIG. 20

zero (16) gives sensibly the minimum permissible resonator gap voltage. For the Glasgow synchrotron, with  $\hat{W}_S = 300$  MeV,  $r_S = 125$  cm,  $\frac{\Omega_s}{2\pi} = 40$  c/s, this is 1.8 kV.

Theoretical considerations of betatron to synchrotron transition 59, 60 current at the time of development of the RF oscillator, indicated that considerably higher voltages than the minimum would be necessary for efficient changeover. On this basis, a total gap voltage of 3.5 kV was catered for i.e. 1.75 kV per resonator. Later treatments 61, 62, 63 indicate that efficient trapping occurs with voltages not greatly in excess of the minimum.

A full account of the resonators is given in reference 64.

Fig. 20 is a block diagram of the RF set which produces 10 kW peak power at 38.2 Mc/s.

Each drive unit contains a tunable, 9.55Mc/s low power oscillator and amplifier giving 10 W CW. This feeds the modulated class C power stages comprising two frequency doublers and a push-pull output stage.

The wattmeter is based on the directional coupler principle 65 and indicates the forward and reflected powers in the resonator feeds.

Provision is made, within the modulator, for shaping of the RF envelope; this is discussed fully in chapter four.

The RF pulse is of six milliseconds duration.



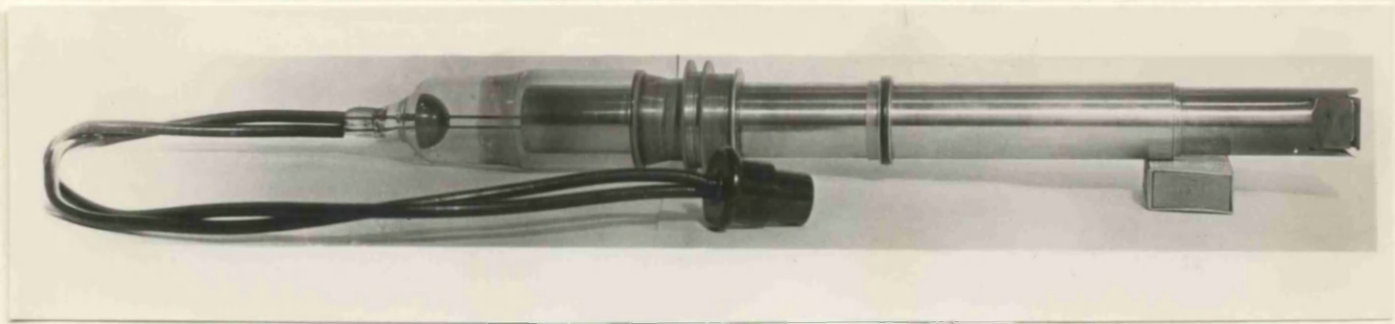
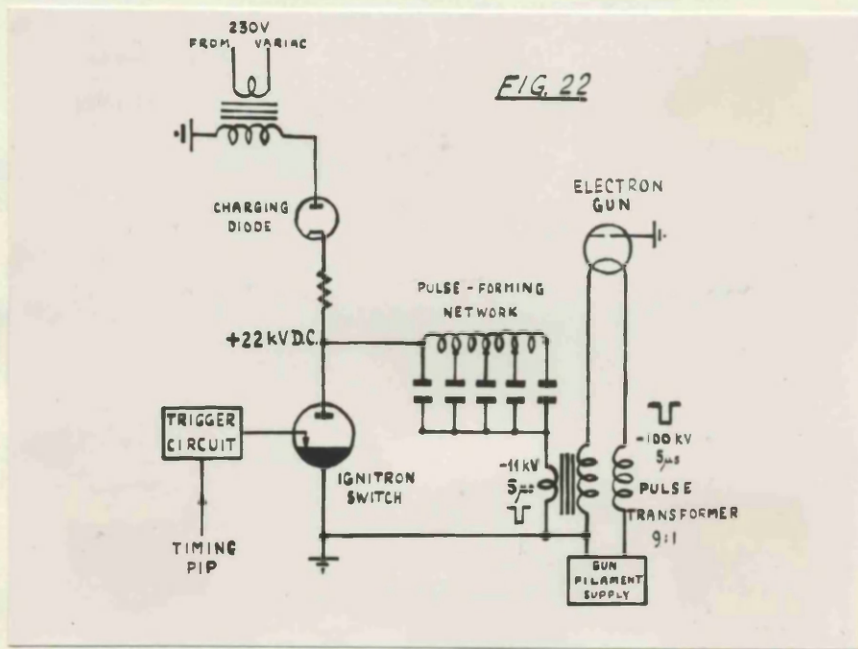


Fig. 21



### 2.5.2 Injector Equipment.

The electrons are injected from a hot-filament gun, an intricate structure of stainless steel and glass - fig. 21. It protrudes into the donut through an O-ring vacuum seal on a port. The gun can be adjusted in position by means of three remotely controlled motors which cater for radial movement in and out of the donut, rotational movement about the gun axis, and movement of the filament with respect to the anode slit. These last two adjustments give very fine control of the angle of fire of the gun.

The stainless steel anode cylinder is earthed and the thoriated tungsten filament is pulsed to a negative voltage to accelerate electrons through the anode slit. Injection voltages up to 100 kV are available, from the modulator sketched in fig. 22. The pulse length is variable from 1.25  $\mu$ s to 5  $\mu$ s in steps of 1.25  $\mu$ s and the filament voltage is adjusted so that the gun emission is  $\sim$ 300 mA as measured between donut coating and earth.

### 2.5.3 Expander Modulator.

The expander modulator produces a current pulse in coils enclosing the poles, which weakens the guide field and displaces the electrons on to a target external to the synchronous orbit.

This displacement is most economically accomplished by means of a step field arrangement, 66, in which the guide field

is reduced over only a portion of the orbit. As a result, forced oscillations of the electron motion are set up and the equilibrium orbit is slightly expanded and shifted towards the region of weaker field.

Another method, requiring more power, is the plus-minus arrangement, 15, in which the guide field is increased over  $180^\circ$  of the annulus and reduced over the other  $180^\circ$ . This just shifts the orbit towards the weak field region, being in effect a combination of two  $180^\circ$  step fields which produce additive orbit shifts and cancelling changes of orbit radius.

An advantage of this second method is that it can be produced by a single coil, as in fig. 23, automatically decoupled from the main magnet field.

Consider an electron of energy  $W$  moving in the guide field

$$H_r = H_0 \left( \frac{r}{r_0} \right)^{-n}, \quad 0 < n < 1 \quad (17)$$

with equilibrium orbit  $r_0$  given by

$$W = 300 H_0 r_0 \quad (18)$$

If the field is weakened so that

$$H_r' = (H_0 - \Delta H_0) \left( \frac{r}{r_0} \right)^{-n} \quad (19)$$

the equilibrium orbit alters to  $r_0 + \Delta r_0$  where

$$W = 300 H_{r_0 + \Delta r_0}' (r_0 + \Delta r_0) \quad (20)$$

A sudden field change would cause the electron to be shock-excited into undergoing free oscillations (section 1.3) about the new orbit, of frequency

$$\frac{r_0}{2\pi} = (1-n)^{\frac{1}{2}} \cdot \frac{c}{2\pi r_0} \quad (21)$$

However, if the weakening takes place gradually, the electron merely moves outwards to the new orbit.

Expansion of (20) to first order incrementals gives, with (18), the relationship

$$\frac{\Delta H_0}{H_0} = K^2 \frac{\Delta r_0}{r_0} \quad (22)$$

where 
$$K^2 = 1 - n \quad (23)$$

Consider now the motion of an electron in a  $180^\circ$  step field viz.

$$H_r = H_0 \left(\frac{r}{r_0}\right)^{-n}, \quad -\pi \leq \theta \leq 0 \quad (24a)$$

$$H_r' = (H_0 - \Delta H_0) \left(\frac{r}{r_0}\right)^{-n}, \quad 0 \leq \theta \leq \pi \quad (24b)$$

$r, \theta$  are the polar coordinates of the particle in its orbit. In one half of the annulus the equilibrium orbit is  $r_0$  in the other  $r_0 + \Delta r_0$ . If the weakening step  $\Delta H_0$  is established (from zero) at a rate slow compared with the period of the free oscillations, these are not induced and the electron undergoes a forced oscillation i.e. a cyclic motion about the mean equilibrium orbit  $r_0 + \frac{\Delta r_0}{2}$ .

By setting  $x$  as the displacement from the normal orbit  $r_0$ , the motion can be represented in the form

$$x = a_1 \cos K\theta + b_1 \sin K\theta, \quad -\pi \leq \theta \leq 0 \quad (25a)$$

$$x = \Delta r_0 + a_2 \cos K\theta + b_2 \sin K\theta, \quad 0 \leq \theta \leq \pi \quad (25b)$$

where the constants  $a, b$  are determined by the continuities of  $x$  and  $\frac{dx}{dt}$  at the points  $\theta = 0$  in (25a, 25b) and  $\theta = -\pi$  in (25a) with  $\theta = +\pi$  in (25b).

Since  $\frac{d\theta}{dt} = \frac{c}{r_0}$  the relationships between the constants are:

$$a_1 = \Delta r_0 + a_2 \quad (26a)$$

$$a_1 \cos K\pi - b_1 \sin K\pi = \Delta r_0 + a_2 \cos K\pi + b_2 \sin K\pi \quad (26b)$$

$$b_1 = b_2 = b \quad (26c)$$

$$a_1 \sin K\pi + b_1 \cos K\pi = -a_2 \sin K\pi + b_2 \cos K\pi \quad (26d)$$

(26c) with (26d) gives

$$(a_1 + a_2) \sin K\pi = 0 \quad (27)$$

Now  $\sin K\pi = 0$ , if  $K\pi = l\pi$ ,  $l = 0, 1, 2, \dots$

i.e. if  $n = 1 - l^2 = 1, 0, -3, \dots$

But it is specified (17) that  $0 < n < 1$ , hence  $\sin K\pi \neq 0$  and

$$(27) \text{ gives } a_1 + a_2 = 0 \quad (28)$$

$$\text{Hence, (26a) with (28), } a_1 = \frac{\Delta r_0}{2} = -a_2 \quad (29)$$

$$(29) \text{ with (26b), } b = \frac{\Delta r_0}{2} \cdot \frac{\cos K\pi - 1}{2} \quad (30)$$

Insertion of (29), (30) into (25) leads to

$$x = \frac{\Delta r_0}{2} \cdot \frac{\cos K(\theta + \frac{\pi}{2})}{\cos \frac{K\pi}{2}}, \quad -\pi \leq \theta \leq 0 \quad (31a)$$

$$x = \Delta r_0 - \frac{\Delta r_0}{2} \cdot \frac{\cos K(\theta - \frac{\pi}{2})}{\cos \frac{K\pi}{2}}, \quad 0 \leq \theta \leq \pi \quad (31b)$$

as the displacement from the normal orbit  $r_0$ , or setting

$$x = y + \frac{\Delta r_0}{2},$$

$$y = \frac{\Delta r_0}{2} \left( \frac{\cos K(\theta + \frac{\pi}{2})}{\cos \frac{K\pi}{2}} - 1 \right), \quad -\pi \leq \theta \leq 0 \quad (32a)$$

$$y = \frac{\Delta r_0}{2} \left( 1 - \frac{\cos K(\theta - \frac{\pi}{2})}{\cos \frac{K\pi}{2}} \right), \quad 0 \leq \theta \leq \pi \quad (32b)$$

give the displacement from the mean equilibrium orbit  $r_0 + \frac{\Delta r_0}{2}$ .

From (32) it is seen that the orbit is displaced towards the

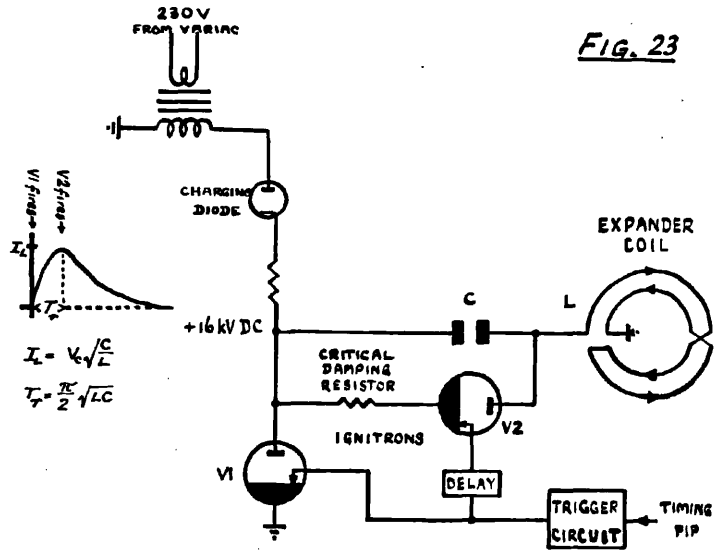
weak field region i.e. towards  $\theta = \frac{\pi}{2}$ , where the displacement

$$\text{is } y_{\frac{\pi}{2}} = \frac{\Delta r_0}{2} \left( 1 - \sec \frac{K\pi}{2} \right) \quad (33)$$

From (22), (33) and relevant magnet data can be calculated the disturbing field required to shift the electrons from the normal orbit on to the target and also



FIG. 23



the power necessary in the coil producing the step field.

The original design produced an optimum step field, using a 3000 amps peak current pulse in a 10  $\mu\text{H}$  coil, obtained by discharge of a capacitor into the coil and damping of the ensuing oscillation at the instant of peak current.

Lack of space between donut and pole faces after installation of the pole face correctors, prevented fitting of this expander coil. A larger area coil was inserted in plus-minus fashion (fig. 23) but the larger inductance,  $\sim 30 \mu\text{H}$ , reduced the current to the insufficient value of 1800 amps. Increasing the capacitor overloaded the rectifier and reduced the charge voltage.

In order to avoid increasing the rectifier power an attempt at redesign was made using the BK24 ignitrons back-to-back as in fig. 12; but as the period of LC oscillation was in this case comparable with the deionization time of the ignitrons, these backfired allowing the capacitor to ring down and discharge completely. This could not recharge sufficiently at the five per second pulsing rate.

Finally, a simplified version of the original form of circuit was used and found to eject electrons at lower peak currents than expected by calculation. This may be due to the establishment of a resonance in the electron motion.

Fig. 23 is a sketch of the modulator.

A plus-minus coil is shown: one half can readily be

disconnected to leave a 180° step field coil; both versions are successful.

The capacitor C charges from the rectifier through the coil. When the BK24 ignitron V1 is fired, C discharges through L, the current rising sinusoidally. At the peak value  $I_L = V_c \sqrt{\frac{C}{L}}$  the ignitron V2 is fired to damp out the oscillatory discharge of C and remove inverse voltage from V1.

#### 2.5.4 Timing Equipment.

The whole sequence of operations i.e. injection, RF on, RF off, orbit expansion, is automatically timed.

A current transformer on the magnet coil centre point, gives a current (or field) waveform as in fig. 13. This is fed into a six-channel multiar box which uses a well-stabilized power pack as reference bias. The power pack voltage and peak voltage of the current transformer output coincide. The multiar 67, 68 is a circuit which indicates equality between a negative-going input voltage and a reference bias voltage. Variation of the bias setting from zero to maximum voltage thus enables selection of any instant of the acceleration interval AB of fig. 13.

Each multiar triggers a blocking oscillator to give out a narrow pulse referred to as a timing pip.

In the original design, the abovementioned operations were catered for by four channels with two channels for



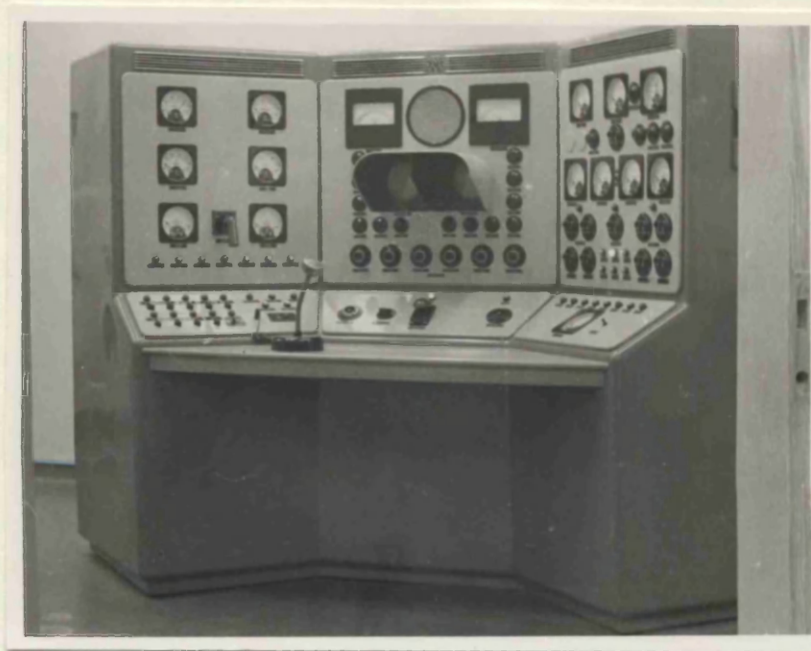
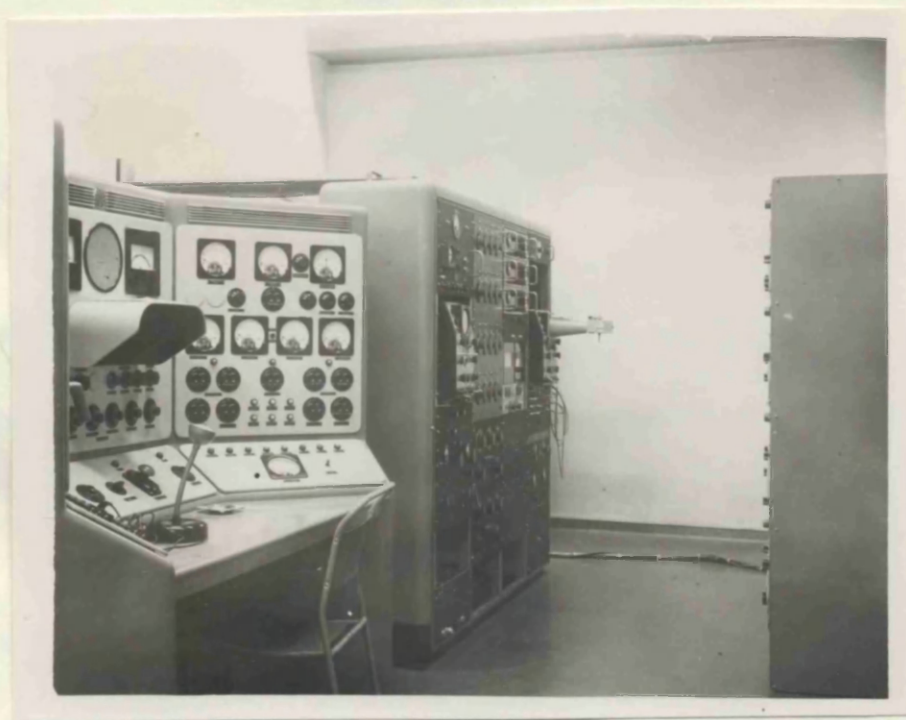


Fig. 24



triggering display units and external equipment.

The injector channel was found to be too jittery for stable injection. DC potentiometer tests showed that the multitar operated over a range of  $\frac{1}{80}$  V. The current transformer peak voltage of 500 V corresponded to a field of 8000 oe. Thus  $\frac{1}{80}$  V  $\equiv$  0.2 oe: at injection the rate of change of field is 0.8 oersted per microsecond (16 c/s) so that the possible injection jitter is  $\frac{0.2}{0.8} = 0.25$   $\mu$ s. American experience at Cornell University had shown that an upper limit of 0.1  $\mu$ s was necessary for a steady beam.

Accordingly the multitar was replaced by a biased peaker strip in the magnet gap, which triggered a blocking oscillator to give the injection timing pip.

## 2.6 Control.

Protection is afforded against electrical power and high energy radiation. All high voltage installations are extensively interlocked to render the apparatus harmless to operating personnel. Automatic fire protection is installed. The magnet is housed in a thick-walled, shielded room below ground level, to contain stray radiation and is operated remotely from a control desk fig. 24: for maintenance purposes it can be operated from the synchrotron chamber itself.

The general layout of the synchrotron is shown in fig. 25. Directly above the beam room and adjacent to the control



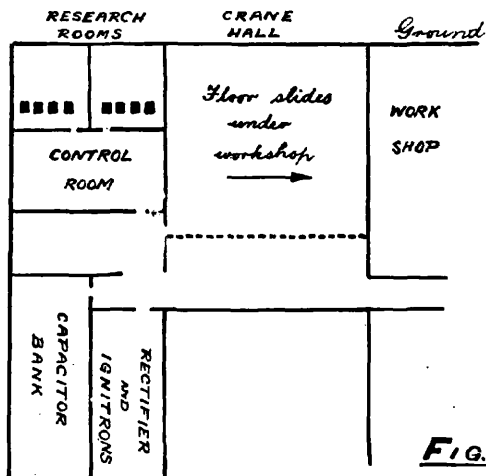
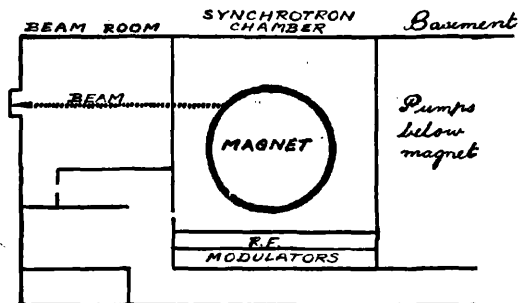


**Fig. 25**

room are research rooms from which experiments can be conducted. Access to the beam is available through ports in the research room floors.

The beam passes through a monitor into a recess of absorbing material - 14 ft concrete - and thence into the earth.

The excitation equipment is situated at a higher level than the magnet, and the coil current is fed down through a fairly long busbar run.

Access to the magnet is obtained by sliding the 130 ton magnet chamber roof under the workshop. Above the magnet chamber is a travelling crane which can handle loads up to 50 tons.

## CHAPTER 3

### THE SEARCH FOR A BEAM

#### 3.1 General Approach to the Problem.

After installation and initial tests of the various component units indicated in chapter 2, an extensive series of magnetic field measurements was undertaken. These included checks on the position of the betatron orbit, symmetry of the field and n-value, and measured the error fields so that the required corrections could be assessed.

The error fields arise mainly from eddy current and hysteresis effects and are thus dependent on the level of excitation of the magnet.

Measurements were taken at various levels by increasing the voltage on the capacitor bank; this being effected by variation of the screen-cathode voltage of the charging pentode in the rectifier set.

However, despite a design figure of 17 kV, the bank suffered extensive breakdown in the region 12-14 kV. Considerable effort and time were expended in search for possible causes of the failure, such as switching transients, before the manufacturers accepted that the capacitors themselves were at fault and new units had to be designed. Repairs to the damaged units permitted temporary running up to 12 kV. The original 190  $\mu$ F units, oil-immersed in steel containers, were to be replaced by 115  $\mu$ F units in the same

size tanks to reduce stress; the consequent increase in number of units called for considerable constructional alterations to the capacitor room.

In the course of these setbacks and delays, preparations were made to expedite the search for a beam.

The general line of attack judged best to follow was to start looking for a beam at low excitation of the magnet, when inhomogeneities are relatively small, and once electrons were successfully trapped into circular orbits, to increase the excitation gradually and bring in field corrections, by trial and error, to maintain a stable orbit.

Further, it was decided to concentrate initially on the betatron phase only, since it was considered that once a really strong betatron beam had been established, transition to synchrotron operation would be fairly easy.

In addition, apart from a very short initial period of operation at the five bursts a second rate, alterations in the capacitor room necessitated use of a temporary excitation system for the magnet.

Accordingly, continuous running at 50 c/s from the mains supply was effected by means of a power transformer. This change eased considerably the visual strain of studying fast waveforms on triggered oscilloscopes, avoided transient conditions in the magnet, and afforded a higher integrated X-ray output from the machine - thus giving increased monitoring sensitivity.

The change back to pulsed operation after a betatron beam had been successfully established presented little difficulty in view of the choice of second half-cycle acceleration (fig. 13) which had been governed by betatron orbit considerations. As the magnet has settled down by the end of the first half-cycle, the field distribution will be very similar to that obtaining under continuous running and little changes in correction will be necessary. On the other hand, the transient conditions occurring initially in the first half-cycle of a magnet pulse give rise to a very different field distribution compared with continuous running and also an undesirable time variation of the betatron orbit.

In view of the above decisions, the number of variable parameters at the start of the search was thirtytwo. This comprised the twentyfour out-of-phase field correctors, the first harmonic corrector (section 2.2.2), the three gun movements (2.5.2), gun voltage, gun emission current, injection timing, and betatron orbit position (2.2.2).

A betatron donut had been installed, similar to the layout of fig. 15 with the resonators replaced by plain sectors. Field measurements had shown that eddy currents in the resonator coatings upset the radial field dependence ( $n$ -value) in the resonator neighbourhood. In keeping with the general plan outlined, of simplification and reduction of variables, it was therefore expedient not to insert the

resonators at this stage.

In these days the sectors were separated by teflon gaskets so that the internal coating of each sector was insulated from its neighbours. Each coating was connected to a common conducting ring through a resistor and the ring itself was grounded through a further resistor, so that monitoring points were available of electron current to individual sectors and total gun emission into the donut.

A gun was installed and aged and the voltage set at 60-70 kV with 200 mA emission. The field correctors were set in the positions giving optimum correction according to measurement, the other parameters were arbitrary.

The search began in August 1953 with the magnet at 600 V excitation and pulsed at five pulses per second. Working from the gun sector, the individual coating current waveforms were observed on a portable oscilloscope and the field correctors were adjusted to encourage electrons to travel round the donut.

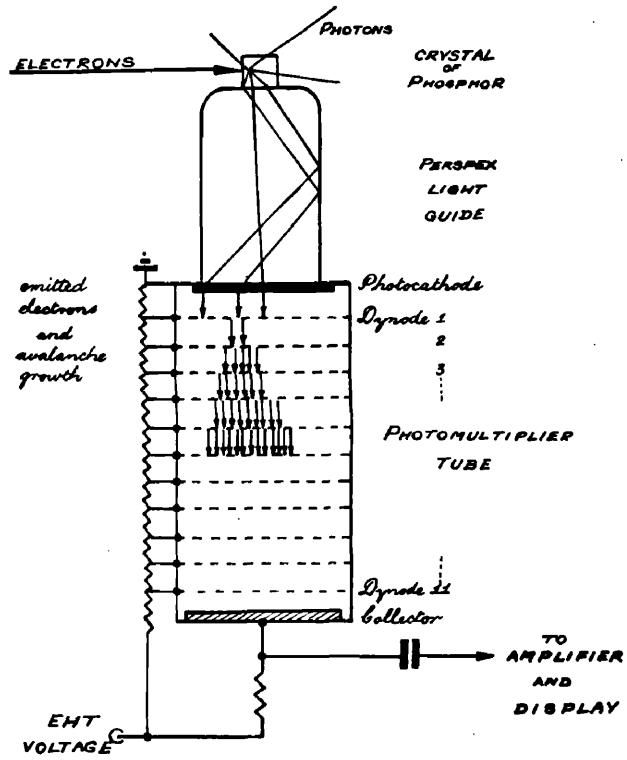
In this way electrons were soon established to circle the donut once. The method of observation was, however, very insensitive and the waveform was badly masked by oscillations due to pick-up from the gun pulse.

It was therefore clear that a more sensitive detector was required before further progress would be made.

Accordingly the internal scintillation probes were brought into use.



**FIG. 26**



### 3.2 Scintillation Probes.

The scintillation probe is an adaptation of the scintillation counter which finds very wide application in many fields of physics.

It consists, fig. 26, of an electron sensitive phosphor mounted on one end of a perspex rod to the other end of which is attached a photomultiplier tube.

When electrons strike the phosphor, its molecules undergo ionization or excitation and photons are emitted in the subsequent return of the molecules to normal state. Some of these light quanta pass down the perspex rod, which acts as an internally reflecting light guide, and fall upon the photocathode of the multiplier tube. As a result, the cathode emits a few electrons which are accelerated to the first dynode by the voltage applied between it and cathode. At this dynode, each incident electron gives rise to further secondary emission electrons, so that the total number of electrons is increased. Each dynode is maintained at a higher potential than the preceding one, so that the multiplication process is repeated, stage by stage down the tube, until a very large bunch of electrons arrives at the collector, giving rise to a workable output voltage pulse. After suitable amplification, this is fed to a display unit.

Common photomultiplier tubes have multiplication factors of  $10^6$ - $10^9$ , cathode to collector, so that it is readily seen that the device is an exceedingly sensitive



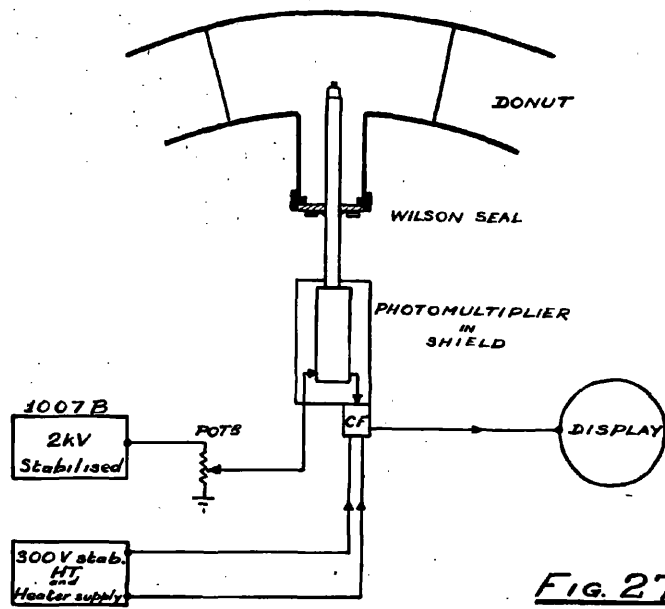


Fig. 27

detector. In fact, with proper choice of phosphor and design of arrangement, single electrons can be detected.

Such a device was developed by the author and employed as an internal beam detector by insertion of the perspex rod into the donut through a vacuum seal as in fig. 27.

Several factors influenced the design of the probe. It was clearly advantageous to have radial movement in order to investigate the beam position and distribution. A Wilson vacuum seal provided this facility.

The phosphor crystal had to be of sufficient size to give a good light yield but thin enough radially to define the beam position reasonably accurately. Crystals of about 1 mm by 1 cm<sup>2</sup> were found to be satisfactory.

In regard to choice of phosphor, the main factors were sensitivity, speed, physical properties and availability. The phosphor had to have high electron sensitivity with preferably low X-ray sensitivity, since it was required to detect the electron beam and not background X-rays from the gun or due to electrons hitting the donut walls; further it had to have much higher sensitivity than perspex or mounting materials.

At injection, electrons circle the donut in  $\sim 5.10^{-8}$  sec so that the decay time of the phosphor had to be  $10^{-8}$  sec, or faster, in order that the pulse height would be sensitive to time variations in the electron beam density.

At the time of commencement of the probe work, the best

available phosphors were zinc sulphide, sodium iodide, and anthracene while the available photomultipliers were RCA 931A (peak response 4000 AU) and EMI 5311 (4600 AU).

Zinc sulphide, silver activated, although most useful for heavy particle detection, is sensitive to large electron fluxes. Its emission spectrum peak is at 4500 AU so that it well matches the 5311 tube. However, its decay time is long,  $10^{-5}$  sec, and it is about equally sensitive to electrons and  $\gamma$ -radiation. Further it is of crystalline powder form and is opaque if used in thick layers. It is stable.

Sodium iodide, thallium activated, is the most sensitive electron detector. The emission spectrum peak is at 4100 AU, well suited to the 931A. Its decay time is  $2.5 \times 10^{-7}$  sec, but it is sensitive to X-radiations because of its high density and the high atomic number of iodine. It is available in transparent crystals which can be readily cleaved to any desired size but is very deliquescent and is normally used immersed in liquid paraffin.

Anthracene, an organic phosphor, has half the electron sensitivity of sodium iodide. It matches the 5311 tube having emission peak at 4450 AU. Its decay time is  $2.7 \times 10^{-8}$  sec; it is relatively insensitive to X-rays. It occurs in clear crystals, readily cut but somewhat volatile at very low pressures.

The RCA 931A is an electrostatically focused, nine stage tube operated at 100 V per stage, or 1000 V overall,

and has a multiplication factor of  $10^6$ . It is somewhat noisy, but is small and inexpensive.

The EMI 5311 is an eleven stage, "Venetian blind" type tube, operated at 2000 V, with multiplication factor  $10^7$ . It is considerably quieter than the 931A, larger, more expensive, and having an end cathode, very suitable for light guide attachment.

References 69-71 give further details of phosphors and tubes.

In view of the above characteristics it was decided to use anthracene in conjunction with a 5311 tube as an internal electron beam detector, and sodium iodide mounted, in a thin-walled perspex box of liquid paraffin, directly on to a 931A tube as an external X-ray beam detector.

Other factors affecting design were the need to protect the photomultiplier from external lighting by suitably enclosing the perspex rod, and also to shield the tube from the leakage magnetic field in the centre of the magnet. Finally the device had to be simple and robust.

A solution to the magnetic pick-up problem was to use a long perspex rod suitably bent such that the photomultiplier could be sited on top of the magnet or well away from it. However this arrangement would have been clumsy to adjust radially and difficult to enclose with few supports on to the rod.

Qualitative experiments with a lamp, ground glass screen,



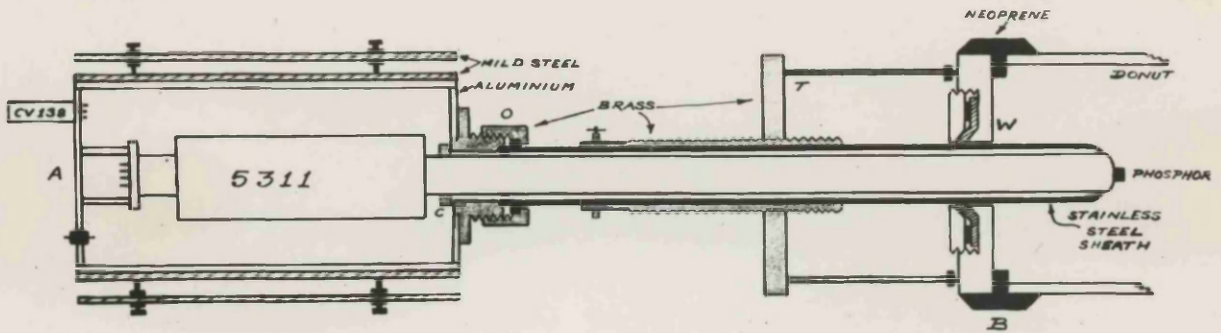


FIG. 28

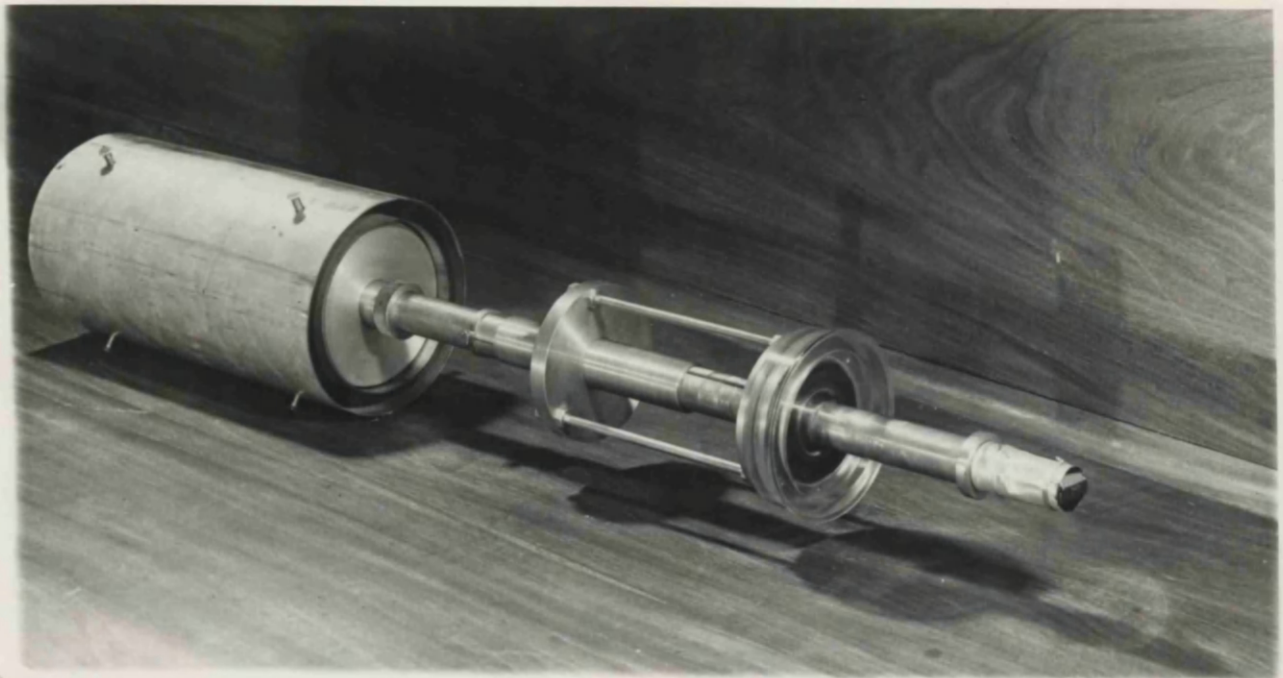


Fig. 29

sections of perspex rod and a photocell had shown that considerable light was lost through the sides of the rod as its length was increased, at joins, or at points of support. Slight loss occurred if the polished surface of the rod had small smears of vacuum grease daubed on it. These effects were less serious with rods of larger cross-section.

In view of these findings, it was decided to use as short a section of light guide as possible and to screen the photomultiplier with mild steel shielding and support the perspex rod light sheath at one place only. Sufficient length of rod had to be used to keep the the metal-work away from the flux bars and the magnet gap in order not to disturb the field.

Accordingly the arrangement of fig. 28 was adopted and, apart from slight modifications discussed later, proved satisfactory.

The 5311 tube and its associated circuits were mounted inside a light-tight cylindrical aluminium can surrounded by two cylinders of  $\frac{1}{8}$  in mild steel acting as magnetic shields. The can was grounded to minimize electrostatic pick-up in the photomultiplier from the injector gun pulse.

As the display units were situated some distance away from the centre of the magnet, the photomultiplier output pulse was fed into a cathode follower unit, using a CV138, incorporated into the main assembly.

EHT supply to the 5311, HT and heater supplies to the CV138, and the output line were brought through the end plate A by means of screened cables. On unscrewing this plate, the whole photomultiplier unit could be withdrawn without disturbing the rest of the assembly.

The perspex rod of 1 in diameter and approximately 30 in length, was enclosed in a  $\frac{1}{32}$  in brass tube of  $1\frac{1}{16}$  in inside diameter, supported by means of the rubber O-ring, which also provided a vacuum seal, so that the rod was clear of the brass tube. A circlip C, cut so that it touched the perspex as little as possible, prevented the rod from being drawn into the vacuum.

The rod was held in contact with the photomultiplier cathode end as shown - a gap here caused diminished output.

In order to minimize beam-disturbing eddy currents, it was desirable to have as little metal-work as possible in the vicinity of the donut. It was, of course, necessary to render conducting the surfaces of the phosphor and extremity of the rod in order to prevent them from charging up and disturbing the electron beam.

With these points in mind, the Wilson seal holder W was made of perspex and the brass sheath was kept thin.

The first probe had the brass O-ring clamp O about four inches from the phosphor end with thin aluminium foil up to the tip which was coated with aquadag. This arrangement was satisfactory at low magnet excitations but as progress was



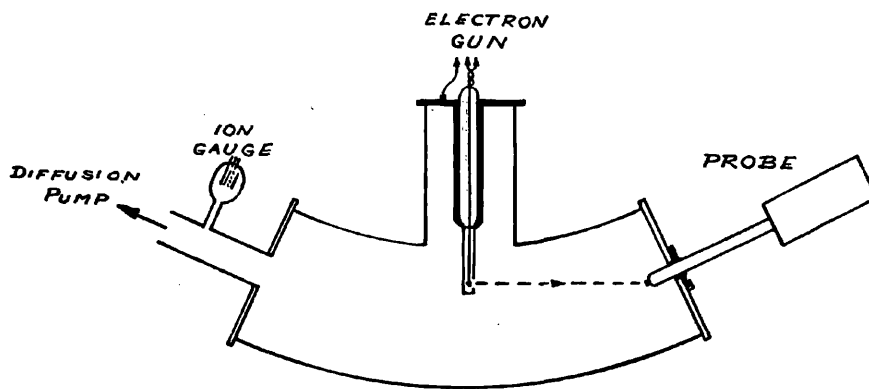


Fig. 30

---

made the design was modified to that of figs. 28, 29 and the brass sheath was replaced by stainless steel.

Attachment to the port sector was made by means of specially moulded neoprene unions B and the Wilson seals were made of  $\frac{1}{16}$  in rubber, the hole being  $\frac{5}{8}$  in diameter. All vacuum joints and seals were slightly greased. The radial position of the probe could be readily adjusted by means of the adjuster T clamped to the sheath.

Before inserting the probe into the donut, it was tested on the bench with a  $\text{Sr}^{91}$  source of  $\beta$ -rays and then in a single port sector, evacuated at one end by a 2-in diffusion pump, fig. 30.

A gun was inserted at the port and lined up to fire at a zinc sulphide screen attached to the other end; this was then removed and replaced by the probe assembly.

This arrangement served to check the vacuum tightness of the device and indicate the type of output waveforms to be encountered.

A 1 mm by 1 cm<sup>2</sup> crystal of anthracene had been cemented on to the end of the rod with Canada balsam and covered with aluminium foil of 0.0002 in thickness - sufficient to stop 25 keV electrons.

When the vacuum pressure reached  $10^{-5}$  mm Hg, the gun was pulsed at 50 c/s (10  $\mu$ s at 20-30 kV) and the output waveforms observed on an oscilloscope. These were shown to be due to electrons hitting the phosphor by

a) deflecting the beam with a permanent magnet,  
b) switching off the gun filament supply, and  
c) reducing the gun HT supply gradually, when a noticeable diminution in pulse height was observed at about 25 kV.

As a result of these tests, the probes were judged free of major defects and considered ready for use. Accordingly one was inserted into the donut behind the gun, its tip covered with 0.001 in aluminium foil - to stop 65 kV electrons, so that, by injecting at about 60 kV, accelerated particles could be detected.

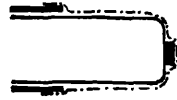
However, the donut pressure, after remaining at  $10^{-6}$  mm Hg for some time, gradually deteriorated to  $10^{-4}$  mm Hg and on removal of the probe, after unsuccessful leak-hunting, the foil was found to have burst and some anthracene had distilled into the donut.

This galling experience was very surprising after the trouble-free single port tests but may have been due to the different manner of evacuation. In the donut the pressure does not fall gradually, as in the bench arrangement, but being automatically sequenced, is subjected to distinct drops in pressure and such a surge may have caused rupture of the foil and exposure of the phosphor surface to the vacuum.

In order to avoid repetition of this occurrence the probe sheath was slightly modified.



FIG. 31



*Mk I Aluminium foil over anthracene.*



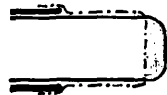
*Mk II Aluminium foil over perspex.*



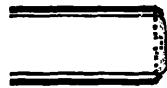
*Mk III Copper foil window over anthracene.*



*Mk IV Perspex cap over anthracene.  
End covered with aquadag.  
Aluminium foil from dag to sheath.*



*Mk V Perspex skin over anthracene.  
Aquadag and aluminium foil.*



*Mk VI Stainless steel sheath.  
Lugs into aquadag  
Plastic phosphor.*

Various arrangements were tried but discarded, in turn, as insensitive until a successful version was made.

The stages of development are shown in fig. 31: perspex alone was tried, covered with aluminium foil at the tip (Mk II). Next, anthracene taped on to the rod, totally sheathed, the end being covered by a 0.002 in copper window let into the brass (Mk III). Mk IV had anthracene enclosed in a perspex cylinder of wall thickness 0.002 in: the whole end of this successful version was coated with aquadag to prevent charging up. Mk V followed logically from it viz., attachment of the anthracene to the perspex rod with perspex cement; when dry, the whole surface of the crystal was painted over with perspex cement thinned down with chloroform so that the phosphor was sealed in a fine skin of perspex. The probe tip was then covered in aquadag.

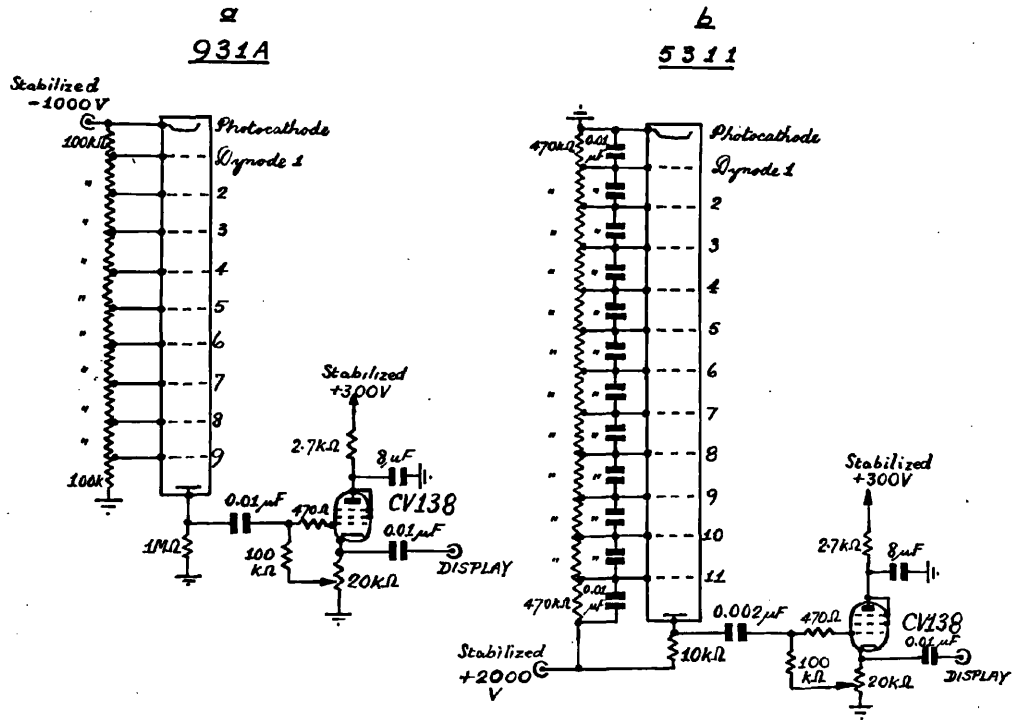
This was the most sensitive anthracene probe, being the nearest possible approach to the bare crystal. Fig. 29 is a Mk V.

Finally, after the anthracene probes had been put to successful use in establishing a betatron beam, plastic phosphors became available and the final Mk VI probes were constructed.

Tetraphenyl butadiene in polystyrene has one quarter the sensitivity of anthracene for electrons, decay time of  $8.10^{-9}$  sec, is available in large clear masses, easily machined and polished. It is stable in a vacuum.



FIG. 32



Cuboids 1 mm by 1 cm<sup>2</sup> were stuck directly on to the rod with perspex cement and coated with aquadag.

The best shape for the end of the rod is obtained by machining a hemisphere and cutting this off flat, normal to the axis of the rod. All light crossing the flat is internally reflected, irrespective of the position of the crystal.

In the Mk IV, V versions, the sheath was of brass and the tip was covered with aquadag; the two conducting portions were joined by aluminium foil suitably punctured to allow the space between rod and sheath to evacuate. The final, stainless steel version dispensed with the foil; lugs on the end of the sheath made direct contact with the aquadag.

Fig. 32 gives the circuits associated with the photomultipliers. The wide-band A1 amplifier of a Cossor 1035 oscilloscope was used as display and the cathode follower was designed to reproduce a very fast falling edge without cutting off.

### 3.3 Use of the Probes to find a Betatron Beam.

As indicated in section 3.1, a "once round" beam had been established by donut coating current observations. A Mk II probe was inserted 25 IX 1953, and the probe output waveforms were examined. As the phosphor was perspex in this case, it was necessary to run the 5311 at maximum voltage and use large oscilloscope gain.

The type of trace observed on the display, which was

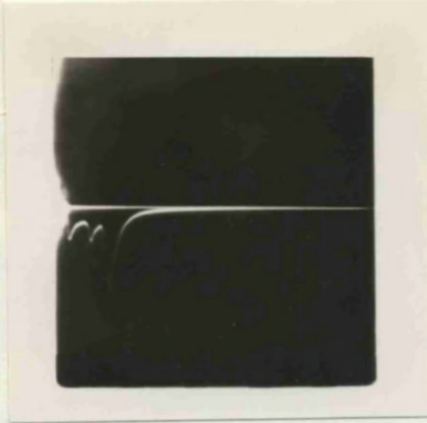


FIG. 33

a

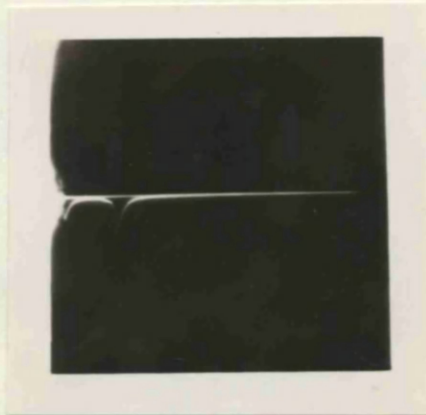


b



NO DC

c



DC  
APPLIED

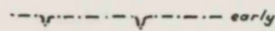
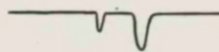
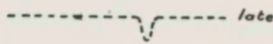
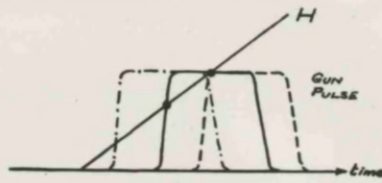


FIG. 34

triggered by a peaker strip in the magnet gap, is shown in fig. 33. For a fixed gun voltage, the probe trace showed the following variation as the injection time was varied from late to early.

At first the timing was too late and no output was observed, then a small pulse appeared which increased in size and width as the timing was made earlier. A second earlier pulse then separated from the larger original and moved away from it in time, the original pulse remaining stationary. As the timing was made earlier still the two pulses diminished in size until no output was visible.

While there were two pulses simultaneously, minor peaks were observed in between: these were to play an important part in the establishment of a beam.

These waveforms, which were due to electrons circling the donut because they varied with gun timing, voltage and emission, are readily explained by fig. 34. As the gun pulse is of finite length, there are in general two instants when the gun voltage exactly matches the field value at that instant (equation (3), section 1.1) and stable injection will be most favourable. Departure from flatness of the pulse top e.g. ringing, may give rise to intermediate matching instants.

The various parameters indicated in 3.1 were laboriously varied in an attempt to encourage a pulse to appear much later on the trace, representing an accelerated beam, but to no avail.



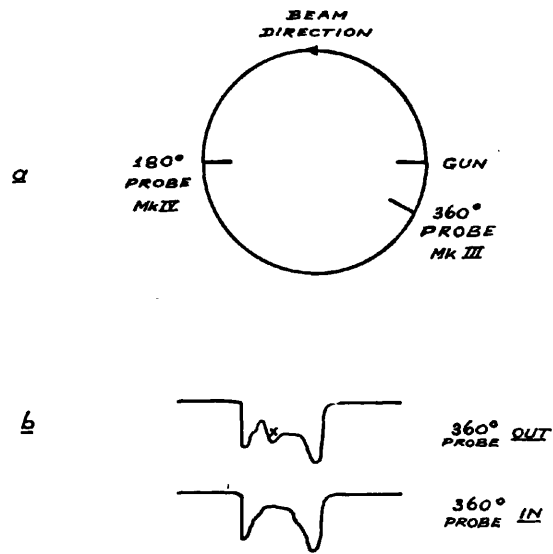


FIG. 35

---

It became clear that either the probe was insensitive or something else was wrong. Accordingly a Mk III probe was inserted but despite the increased sensitivity, no further progress was made. The magnet top was lifted and the donut was removed for inspection.

Several bare patches which had developed on the internal coating, near the gun, were painted over with aquadag. Some of the teflon gaskets were found to be protruding into the donut, so to prevent their charging up all gaskets were coated with aquadag, except those in the vicinity of the gun. Being subjected to the most intense electron bombardment, these were wrapped in aluminium foil.

A Mk IV probe had been made ready and the double probe arrangement of fig. 35a was put together on reassembly.

One probe was inserted opposite the gun and another just behind the gun. The first was called the  $180^\circ$  probe and the other the  $360^\circ$  probe although this was strictly  $324^\circ$  round the orbit from the gun; the gap of two sectors reduced direct electrostatic pick-up from the gun.

With this arrangement it was hoped to discover if the beam were going round the donut more than once.

Both probes were set at a nominal radius of 120 cm and the magnet correctors were adjusted to build up an intermediate peak (x, fig. 35b) of the  $180^\circ$  probe waveform. When this was of maximum size, the  $360^\circ$  probe was moved gradually into the donut.



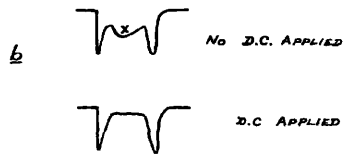
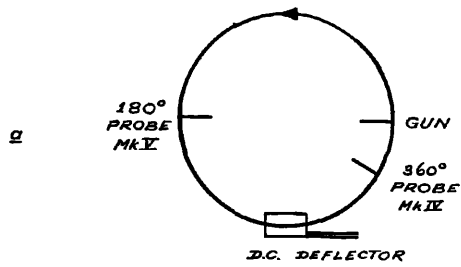
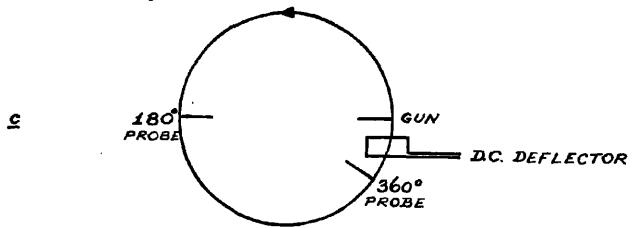


FIG. 36



The central portion, x, of the  $180^\circ$  probe waveform was observed to disappear - it therefore corresponded to electrons which were going round the donut at least one and a half times. After two months of tedious variation of magnet parameters, this was an encouraging result - 2 XI 1953.

At this stage, the change was made to continuous 50 c/s magnet excitation and the donut assembly was altered to the arrangement of fig. 36a, involving a change to more sensitive probes and the addition of a DC deflector coil between the probes. This coil consisted of a few turns wound round the back limb of a cee. On passing a direct current through the coil, a bias field was set up in the cee which prevented electrons from travelling beyond that point of the donut.

Work recommenced at 600 V, 50 c/s excitation.

With the  $180^\circ$  probe set at 119 cm radius and the  $360^\circ$  probe pulled clear into its port, the magnet was tuned for maximum "one and a half times round" electrons as observed on the  $180^\circ$  probe, the DC deflector being used to wipe out the central portion of the trace (fig. 36b, cf. figs. 33b,c).

The next step consisted in putting the DC coil between the gun and the  $360^\circ$  ( $324^\circ$ ) probe as in fig. 36c.

With both probes at 119 cm radius, the two output traces were displayed together. It was observed that the central portion of the  $360^\circ$  probe trace vanished simultaneously with that of the  $180^\circ$  probe on application of the DC deflector current. Thus electrons had been established as circulating



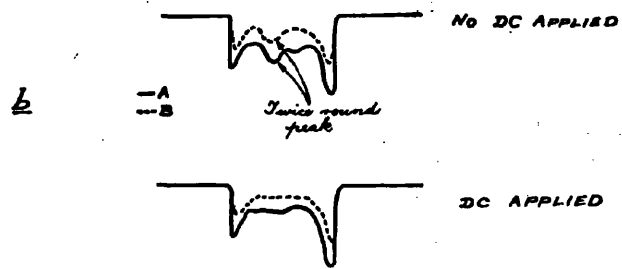
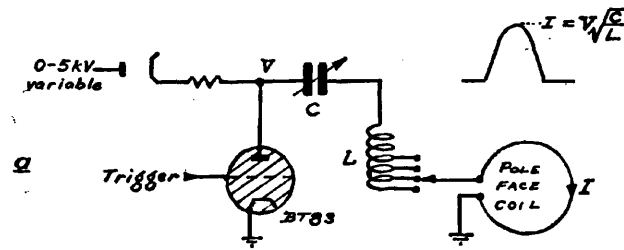


Fig. 37

the donut twice.

At this stage both probes had been converted to the most sensitive Mk V version.

In order to provide a means of expansion of the orbit, one of the poleface coils, fig. 11, was connected to a current pulse modulator, fig. 37a.

The modulator was triggered at injection, at a rate less than 50 c/s so that it was possible to observe the probe traces, corresponding to the normal and expanded orbits, in superposition, as in fig. 37b.

With the modulator switched off, a twice round peak was tuned up on the  $360^\circ$  probe by use of the DC deflector. This is A in fig. 37b. On switching on the orbit expander modulator, the disturbed trace was observed. This still had a twice round peak B, identifiable with the DC deflector. The difference between the two traces therefore corresponded to electrons which had circulated more than twice round the donut, and which missed the probe when the orbit was expanded. As an additional check, the connections to the poleface coil were interchanged in order to contract the orbit when the modulator was triggered. The once round trace then showed an extended tail which vanished when the DC deflector was operated.

Hence it was concluded that electrons were definitely circulating the donut many times, but as no delayed pulse was ever seen, it was clear that they were not trapped in



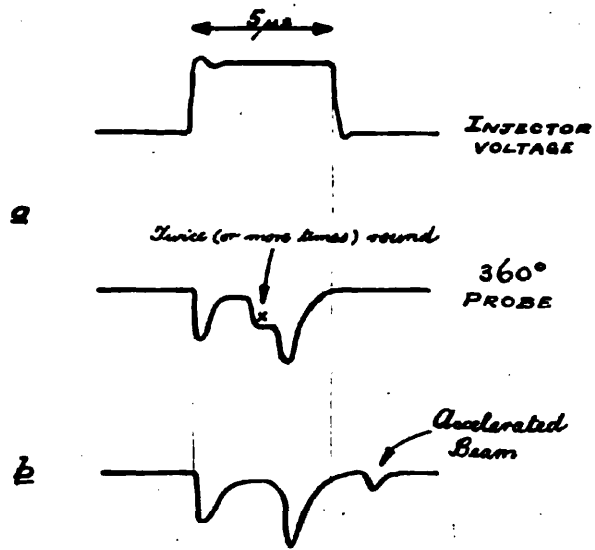


**FIG. 38**

stable orbits but were peeling off to the walls.

The modulator was restored to act as an orbit expander and a delay was incorporated into its trigger circuit to give variable operation at any instant from injection onwards.

A "twice or more times round" beam was maximally tuned by observation of the  $360^\circ$  probe trace and use of the DC deflector. This beam was made to occur as late as possible and was displayed simultaneously with the injector gun pulse fig. 38a.

The orbit expander was then triggered and its timing and rate of change of current were varied to provide various rates of orbit expansion. After some experimentation, the twice round pulse was moved out beyond the back edge of the gun pulse, fig. 38b. As this delayed pulse varied with gun voltage and timing and disappeared when the DC deflector was operated, it represented a tiny accelerated beam.

Variation of the magnet parameters enabled this pulse to be built up and as its size increased, it moved out from the gun pulse eventually occurring some  $10 \mu\text{s}$  after the gun trailing edge. (13 XI 1953).

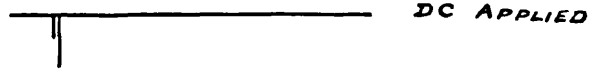
The emerging beam was still present when the magnet excitation was raised, first to 800 V, then to 1000 V, but it became difficult to coax it away from the gun pulse at 1000 V and it was observed to have a marked tail, indicating that unstable conditions persisted.



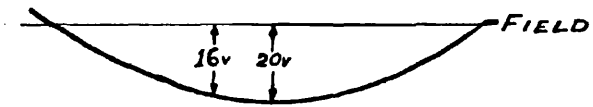
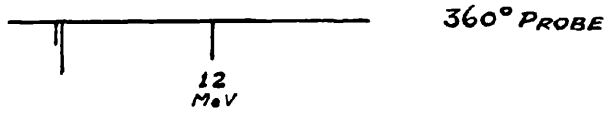
a



360° PROBE



b

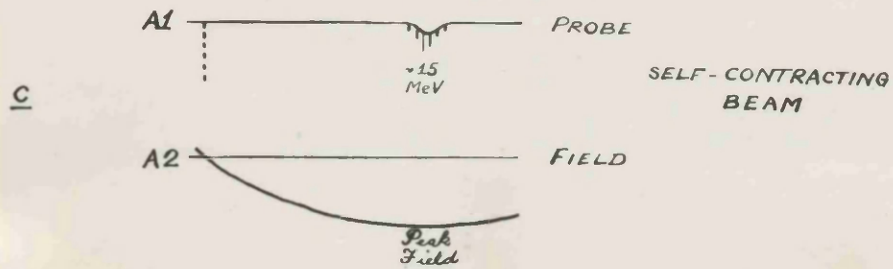
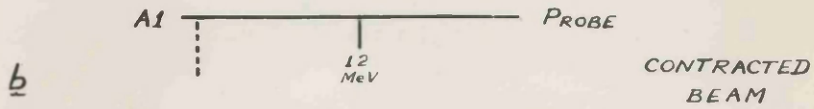
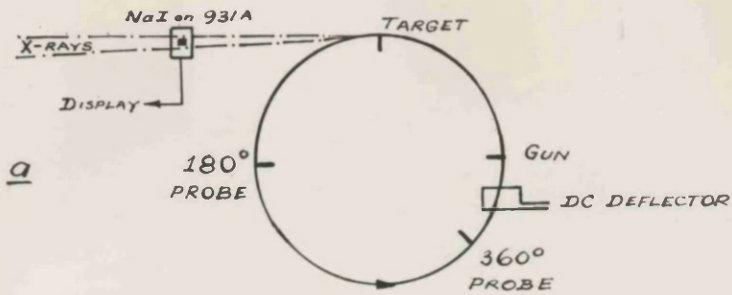


(500V  $\cong$  10,000 oe  $\cong$  375 MeV)

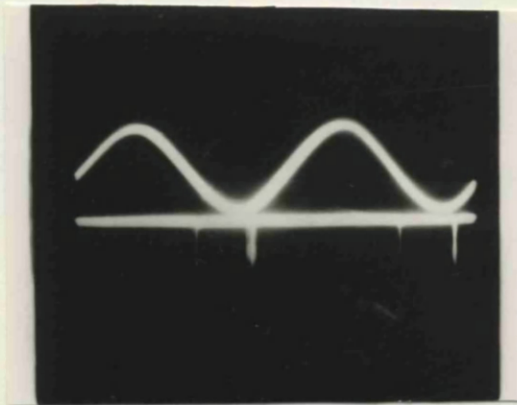
FIG. 39



FIG. 40

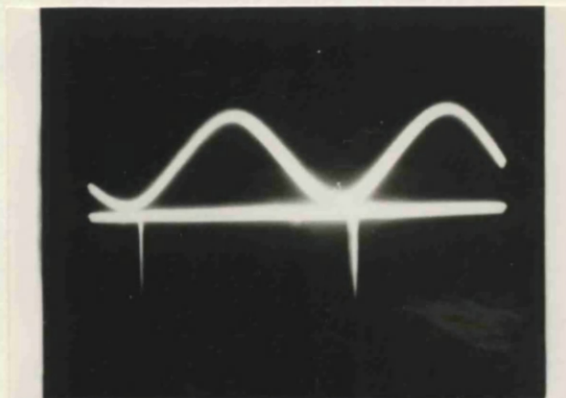


d



FIELD  
INTERNAL  
PROBE

e



FIELD  
EXTERNAL  
DETECTOR

It was therefore decided to bring the poleface n-value correction coils into use and accordingly the two central ones on each poleface were connected up as in fig. 11. The poleface coil used as an orbit expander was changed to become an orbit contractor.

With the magnet excitation back at 800 V and the orbit contractor delayed well after injection, but before peak field, the  $360^\circ$  probe trace was studied (119 cm radius) while the currents to the poleface coils were varied. Almost immediately a pulse appeared, well away from the gun pulse, as in fig. 39a, and it vanished on operation of the DC deflector.

The magnet was then tuned up and all other parameters varied to increase the size and steadiness of this beam and also to bring it out further towards peak field. As progress was made the excitation was increased until finally the beam was obtained at 2000 V on the magnet, the maximum applicable with the temporary 50 c/s system.

The  $360^\circ$  probe was then observed simultaneously with the magnet field waveform (fig. 39b) and the maximum electron energy attained, with use of the delayed orbit contractor, was estimated at  $\sim 12$  MeV. (18 XI 1953).

An internal target of tungsten was inserted into the donut, fig. 40a, and one of the 931A tubes with attached sodium iodide scintillator was sited to detect an X-ray beam from the target.

With the internal probes pulled well into their ports, the external beam was observed and the magnet was tuned up to increase its steadiness.

The orbit contractor was switched off and X-rays of energy  $\sim 15$  MeV were observed at peak field, but not as a concentrated beam, fig. 40c. (19 XI 1953).

As the sodium iodide crystal had been covered with 0.002 in aluminium, no X-rays were observed due to untrapped low energy electrons. On removal of this foil, X-ray pulses at injection were also observed (dotted in fig. 40).

Figs. 40d,e are photographs of the internal and external probe waveforms, (orbit self-contracted), showing the internal betatron beam and output X-ray beam. These traces were taken when more poleface correctors had been put into use to give a concentrated beam after peak field.

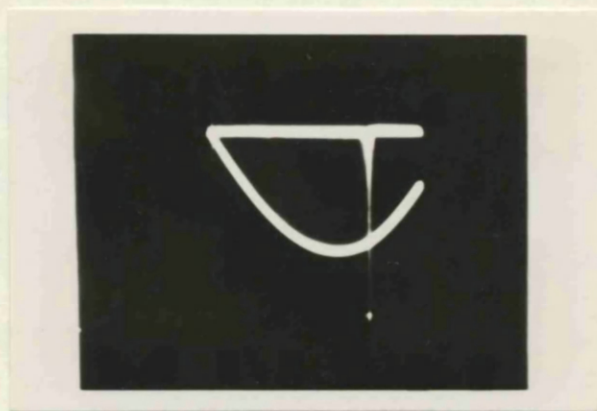
The first phase of the search for a beam was now completed. A betatron beam had been established within three months from the start, largely by study of the effect of laborious trial-and-error variation of the magnet and gun parameters on the internal probes.

This period had seen some false scents - waveforms had been observed which apparently indicated an accelerated electron beam, but which were traced to electronic troubles after rigorous tests - and had been punctuated by stoppages due to the inevitable vacuum troubles and electronic failures.

It was now decided to install the resonators and



Fig. 40f



*PROBE*

*FIELD*

regain the betatron beam, and while this change was taking place, X-ray monitors were fitted to indicate the beam intensity.

The search recommenced in December 1953 with a synchrotron donut, as fig. 15, and the betatron beam was rapidly regained after appropriate readjustment of the out-of-phase field correctors, especially those on cees in the neighbourhood of the resonators. Gradually more of the poleface correctors were connected up until all five on each poleface were in use. By careful adjustment of all parameters, the betatron beam was built up to an intensity of 0.1 roentgen/min at 1 metre from the target. This measurement was obtained by exposure of a 25 r Victoreen thimble, sheathed in a  $\frac{1}{8}$  in cylinder of lead, to the beam.

The self-contracting betatron beam now occurred after peak field as a narrow concentrated pulse fig. 40f.

The injector gun had been run at an emission of 200 mA into the donut, with HT ~70 kV, above which voltage it suffered frequent internal breakdown. While the output was steady, a number of experiments on the variation of output with gun voltage, gun emission and pulse length was carried out. These are reported in chapter five.

At the end of the month the gun was triggered at five pulses per second with the magnet running at 50 c/s.

This was accomplished by feeding the peaker pulse into a 1009B scaling unit and using the pulse at one of the decade anodes to trigger the gun modulator. In this way, some experience was gained with the integrated output reduced by a factor of ten, prior to returning to normal pulsed operation of the magnet.

Early in January 1954, alterations to the capacitor room were completed and the 115  $\mu$ F units were ready for pulsed excitation.

In order to have approximately the same peak current as in the 50 c/s case, the rectifier voltage was set at 2000 V and only three capacitors per leg were put into circuit. The excitation could then be increased by raising the voltage on the bank and by adding further active units - fine and coarse control.

The beam hunt recommenced at the 5 pps rate with all parameters set at the optimum positions before changeover, but no beam was to be found.

A return was made to 50 c/s working with the same result. After a very thorough check of every item of equipment in use, no explanation of this total loss of the beam transpired, so the search had to be started from the very beginning again.

However, the process of adjustment of parameters for maximal indication on the internal probes of once round, twice round, followed by the extraction of the accelerated

beam with the orbit shifter, as outlined above, enabled the establishment of a new beam to be made within a few days. This beam was eventually built up to the best previous intensity, and still obtained when a second change-over to pulsed excitation took place.

Gradually the excitation level was raised and with it the beam energy. As this proceeded, the self-contracting beam, fig. 40f, began to occur before peak field, since the betatron flux bars were now saturating.

Henceforth the beam was observed by contracting it on to the  $360^\circ$  probe at an energy of 5 MeV, (this being the transition energy for 300 MeV operation), by firing the orbit modulator (section 2.5.3) connected as a contractor, at the appropriate field value.

This work continued until the capacitor voltage reached 8 kV.

On 3rd February 1954, one resonator was driven by the RF oscillator for a short time and the 5 MeV betatron beam was converted to a 135 MeV synchrotron beam, occurring somewhat before peak field.

Operations were temporarily halted while running tests between 8 kV and 17 kV were made on the capacitor bank. After satisfactory completion of these tests, observation of the 5 MeV betatron beam was resumed and the magnet excitation gradually raised further, by addition of capacitor units, until it reached full value.



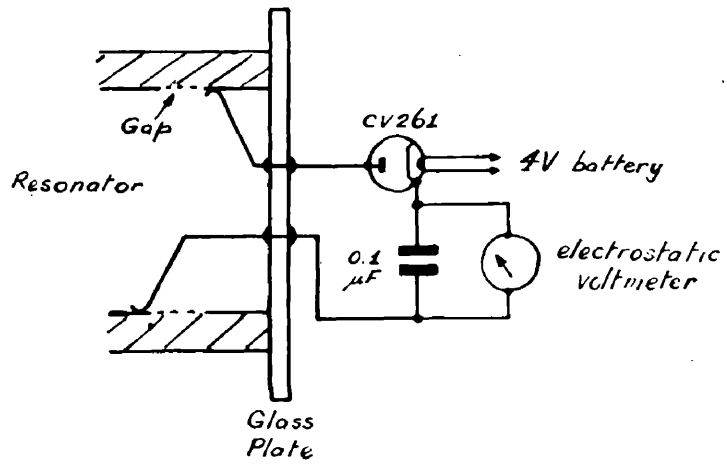


FIG. 41

### 3.4 Synchrotron Operation.

Before the two resonators were installed in the donut, after successful establishment of a betatron beam, they were tested on the bench.

The RF transmitter was tuned up for maximum power output, feeding into resistive dummy loads. One of these was then replaced by a resonator and the peak voltage developed across the accelerating gap was measured with the diode voltmeter of fig. 41. The resonator was continuously evacuated.

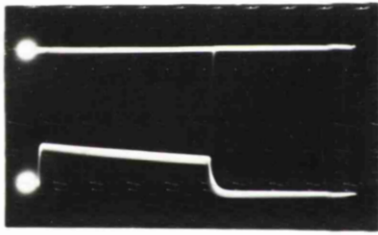
With the transmitter set at 38.2 Mc/s, the position of the resonator feed was adjusted to give the best match as indicated by the incident and reflected power readings of the wattmeter. Also the resonator was tuned to 38.2 Mc/s by moving a short copper strip along the tuning tongue to the position giving maximum voltage on the diode voltmeter. The strip was then affixed to the resonator with tape.

Each resonator was adjusted alone and arranged to have a peak voltage of 2000 V across the gap. Both were then fed in parallel and the transmitter was readjusted. They were then installed in the donut.

As the two accelerating gaps are separated by a short distance, it is necessary that there be a slight phase difference between the two gap voltages at any instant, so that the electrons experience maximum additive accelerating



FIG. #8



PROBE

RF. DETECTOR

┌---6ms---┐

effects in passing through them.

This was accomplished experimentally while the machine was running as a synchrotron by the insertion of an extra length of RF cable into one resonator feed. The beam was observed on the  $360^\circ$  probe, contracted there by the orbit modulator, and short lengths of cable were added to one RF feed until the probe signal was best.

As anticipated, no great difficulty was experienced in converting the betatron beam into a synchrotron beam. It was merely necessary to tune up a good betatron beam and then switch on the RF pulse, adjust its amplitude and time of initiation, and the output pulse observed on the probe would be seen to jump to the end of the RF pulse, fig. 48.

The "RF on" timing is not very critical and some electrons are lost from the beam during transition - this will be discussed in chapter four.

300 MeV synchrotron output was first obtained on 23 IV 1954. At the present time (October 1954) the beam intensity is  $\sim 700$  r/min at one metre from the target and the peak energy is  $\sim 335$  MeV. The intensity measurement was obtained with Victoreen thimble chambers; the energy was estimated from peak field measurement.

Higher intensities yet are expected from this machine by increasing the injection voltage, cf. section 5.1. The present guns are limited to  $\sim 70$  kV, above which frequent

internal breakdown occurs; new guns capable of reaching the available 100 kV are being developed.

Two targets are available, at smaller and larger radii than the synchrotron orbit respectively.

With the use of the expander modulator of section 2.5.3,

the beam can be expanded on to the external target to produce a very short pulse of X-rays,  $\sim 1 \mu\text{s}$ , at any instant of the synchrotron phase up to peak field. The RF is turned off simultaneously with the firing of the orbit modulator.

The internal target is used to produce a slightly longer X-ray pulse. If the RF is turned off somewhat before peak field, the electrons spiral inward, owing to loss of energy by radiation, and strike the internal target.

Much longer X-ray pulses can be obtained if the RF voltage dies away slowly - this is discussed in chapter four.

During this period, the Mk VI probes with plastic phosphors were used.

### 3.5 Intensity Measurements.

The X-ray intensity measurements have been taken with standard 25r Victoreen thimble chambers sheathed in  $\frac{4}{8}$  in lead cylinders. These are charged up to a standard voltage in an instrument designed for the purpose, and then exposed to the beam for a measured time at a known distance from the target. The loss in charge indicates directly the X-ray dosage at the point of measurement and by use of the inverse

square law the intensity at one metre from the target can be ascertained. This is expressed in roentgen per minute or sometimes in r per X-ray burst, by invoking the pulsing rate.

The position of the beam was located with external 931A detectors as already described.

An ionization chamber identical to that used at Cornell University 72 has been constructed for monitoring the beam. This is at present used as an instantaneous monitor calibrated from Victoreen measurements.

Under construction is a double-focusing electron pair spectrometer with which the energy spectrum of the X-rays will be ascertained and then the chamber can be absolutely calibrated.

A health monitor, type 1006, comprising an ionization chamber and associated circuits, is used to give indication of instantaneous and integrated output radiation.



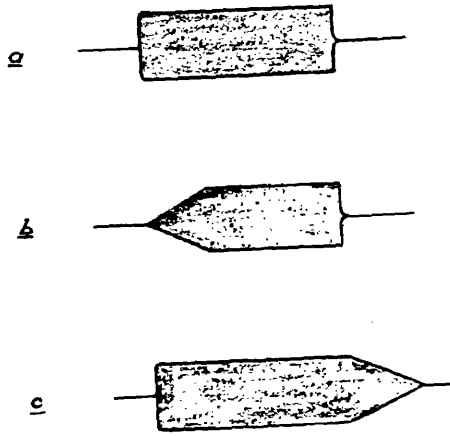


Fig. 42

## CHAPTER 4

### RF SHAPING EXPERIMENTS

#### 4.1 Introduction.

The RF accelerating voltage applied to the resonators at the end of the betatron phase, originally had a square envelope, as fig. 42a, and with such the synchrotron beam was established.

By slowing down the rate of decay of the RF voltage, fig. 42c, a wide X-ray pulse can be generated - this is very useful in coincidence work. If the RF is turned off rapidly just before peak field, the electrons lose energy by radiation and spiral quickly on to the internal target. An estimate of the duration of this X-ray pulse can be made as follows - the symbols have their usual meanings:-

Equation (1) with  $v \rightarrow c$  gives

$$W = e H r \quad (34)$$

The field radial dependence is

$$H = H_0 \left( \frac{r}{r_0} \right)^{-n}, \quad 0 < n < 1 \quad (35)$$

from which

$$\frac{\partial H}{\partial r} = -n \frac{H}{r} \quad (36)$$

Differentiation of (34) with (36) leads to the rate of contraction of the orbit:

$$\frac{dr}{dt} = \frac{\frac{1}{e} \frac{dW}{dt} - r \frac{\partial H}{\partial t}}{H(1-n)} \quad (37)$$

Near peak field,  $\frac{\partial H}{\partial t} \approx 0$ , so (37) reduces to

$$\frac{dr}{dt} = \frac{\frac{1}{e} \cdot \frac{dW}{dt}}{H(1-n)} \quad (38)$$

The energy loss per revolution of the electron by radiation is given by, 83,

$$W_t = \frac{4}{3} \pi \frac{e^2}{r} \left( \frac{W}{mc^2} \right)^4, \quad W \gg mc^2 \quad (39)$$

This is ~500 eV for 300 MeV electrons in an orbit of 125 cm radius.

Now 
$$W_t = \frac{2\pi r}{c} \cdot \frac{dW}{dt} \quad (40)$$

hence, from (38), (39), (40),

$$\frac{dr}{dt} = \frac{2ce}{3\pi^2 H(1-n)} \left( \frac{W}{mc^2} \right)^4 \quad (41)$$

The duration of the X-ray pulse,  $t$ , is the time taken for the electron beam to sweep radially across the target.

If  $x$  is the radial spread of the beam,

$$t = \frac{x}{\frac{dr}{dt}} \quad (42)$$

$x$  is estimated as being 1-2 cm. Setting  $x = 1$  cm gives

$$t = \frac{3\pi^2 H(1-n)}{2ce} \left( \frac{mc^2}{W} \right)^4 \quad (43)$$

Substitution of values ( $H = 8000$  oe,  $r = 125$  cm,  $n = 0.7$ ,  $W = 300$  MeV,  $mc^2 = 0.5$  MeV,  $e = 4.8 \times 10^{-10}$  esu,  $c = 3 \times 10^{10}$  cm/s) gives  $t \approx 30$   $\mu$ s. The observed width is ~50  $\mu$ s.

If the RF voltage decays slowly, the radiation loss is partly offset, so that  $\frac{dW}{dt}$  is diminished; the collapse of the orbit proceeds more slowly and a wide X-ray pulse is obtained.

Several theoretical treatments 59-63 of the electron motion at the time of betatron to synchrotron transition have been made, with results which suggest that the rate of rise of the RF pulse may influence the number of electrons



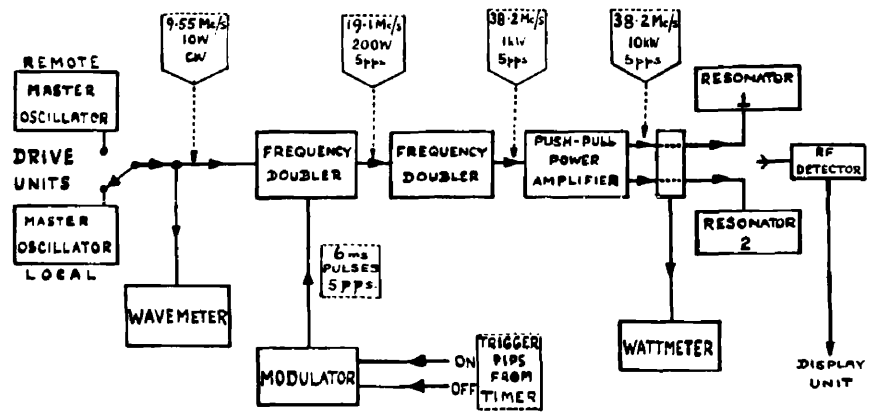


FIG. 20

which are successfully trapped into the synchronous orbit. The electrons begin to undergo phase and concomitant radial oscillations (section 1.4) as soon as the RF voltage is applied to the resonator. Bohm and Foldy 4 show that the amplitude of these oscillations is proportional to the fourth root of the peak gap voltage and inversely proportional to the fourth root of the cube of the electron energy.

Many particles undergo large, unstable oscillations and strike the donut walls or the gun, if the RF voltage is suddenly applied at full amplitude, merely as a result of unfavourable initial transit of the accelerating gap when the voltage there is large. However, if the RF voltage is turned on slowly, fig. 42b, the induced initial oscillations should be smaller in amplitude, while the damping with rising energy should counteract the effect of increasing gap voltage so that more particles might be trapped.

The RF voltage must rise sufficiently rapidly, nevertheless, to supply the electrons with enough energy to remain on the orbit.

With these considerations in mind, the author decided to provide a means of varying the shape of the RF pulse envelope.

#### 4.2 RF Front Edge Shaping.

Fig. 20 is a block schematic of the RF transmitter which consists of a low-power master oscillator and buffer



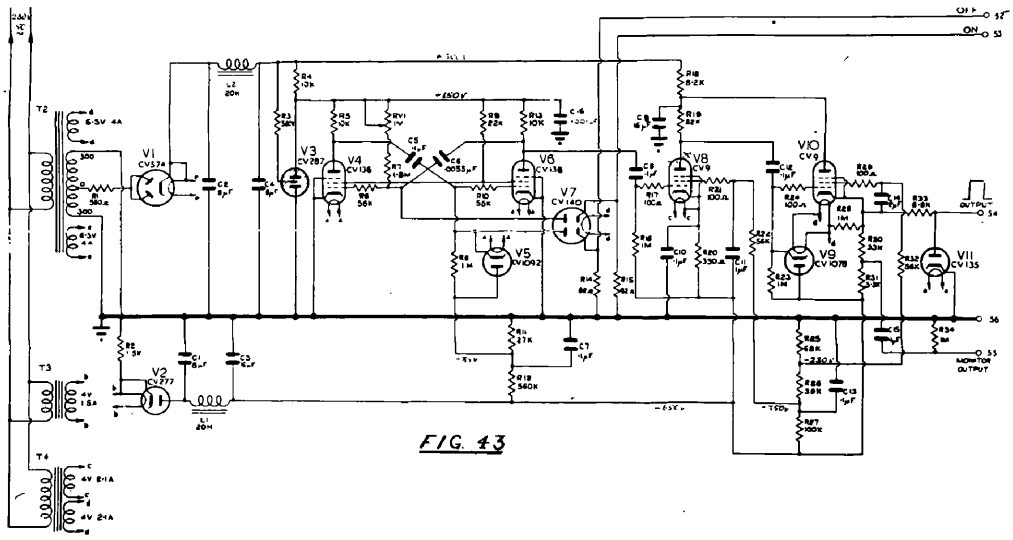


FIG. 43

amplifier, followed by three class C power stages of which the first two are frequency doublers. The master oscillator is tunable about the nominal frequency of 9.55 Mc/s and the whole device is capable of producing 10 kW peak power at 38.2 Mc/s.

In the original design, square wave modulation took place at the control grid of the first doubler stage, by means of the modulator shown in fig. 43.

The triggered multivibrator, valves V4, V6, produced a negative-going square pulse at the anode of V6 which, after amplification by V8 was fed via the cathode follower V10, as a positive-going pulse of some 600 V amplitude, to the grid of the frequency doubler to drive this valve above cut-off. Component values had been chosen to give the pulse the steepest possible sides.

The envelope of the voltage oscillations in a tuned resonant circuit, of quality factor  $Q$ , to which is applied at the resonant frequency  $f$  an ideally square RF pulse, builds up with time-constant  $\frac{Q}{\pi f}$ .

Thus the most rapid time of rise of the RF pulse in the tuned circuit is approximately  $\frac{5Q}{\pi f}$  seconds, and is about 8  $\mu$ s for a resonator of  $Q = 200$  at  $f = 38.2$  Mc/s.

In general, the voltage in the tuned circuit tends exponentially to follow the input variation; specifically if the applied RF pulse rises to full value according to the relation



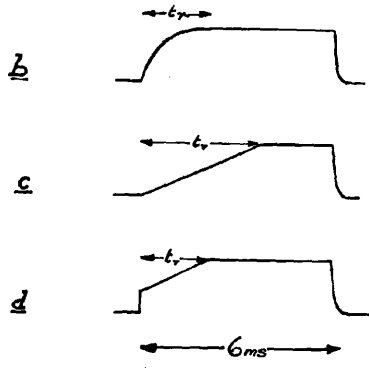
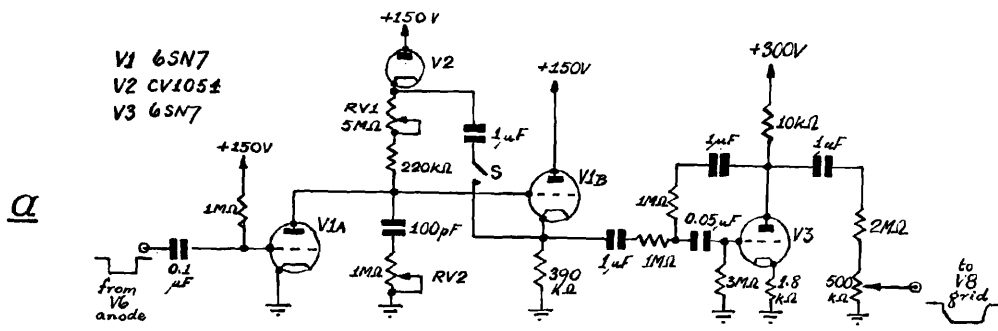
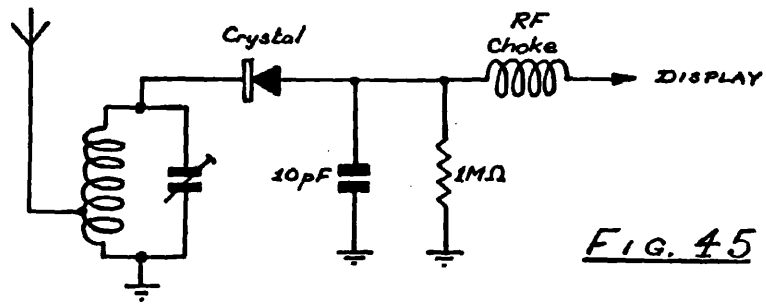


FIG. 44



$$v = V f(t) \sin(\omega t) \quad (44)$$

then the tuned circuit response is approximately of the form

$$v = V' f(t) \sin(\omega t) \cdot (1 - e^{-\frac{\omega}{Q}t}) \quad (45)$$

Thus, if the modulator pulse rises slowly, the RF envelope will also undergo a slow rise. This will not quite be of the same form as the modulator pulse due to the time-constant effect of the resonator and also the non-linearity of the class C stages.

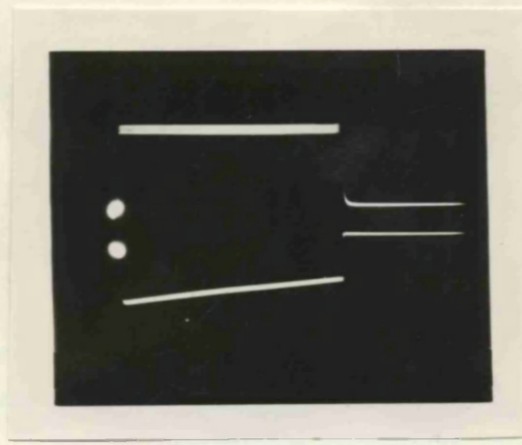
It was therefore decided to investigate the possibility of effecting controllable variation of the RF envelope by shaping the modulator pulse.

This was most conveniently done by insertion of the shaping circuit of fig. 44a between the multivibrator valve V6 and the amplifier V8 of the original modulator, fig. 43.

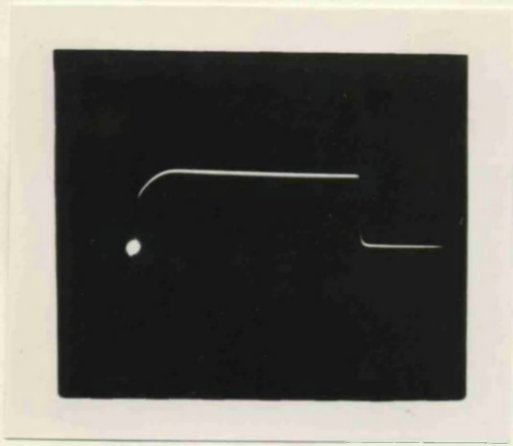
The shaper consisted of a bootstrap V1 and anode follower inverter stage V3. With the switch S open, the front edge of the modulator pulse rose exponentially, fig. 44b, and with S closed, it rose linearly as fig. 44c. Times of rise,  $t_r$ , up to ~6 millisecond were obtainable by variation of RV1. An initial step could be introduced by means of RV2; fig. 44d.

An RF detector unit, fig. 45, was used to display the RF envelope at the resonator input feeds - it was not possible to observe the gap voltage directly with the resonators installed in the donut.

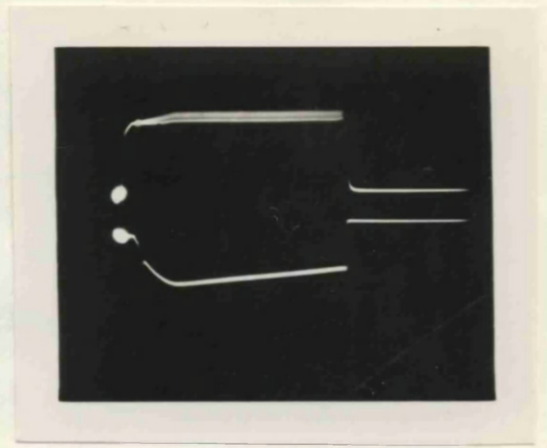




a



b



c

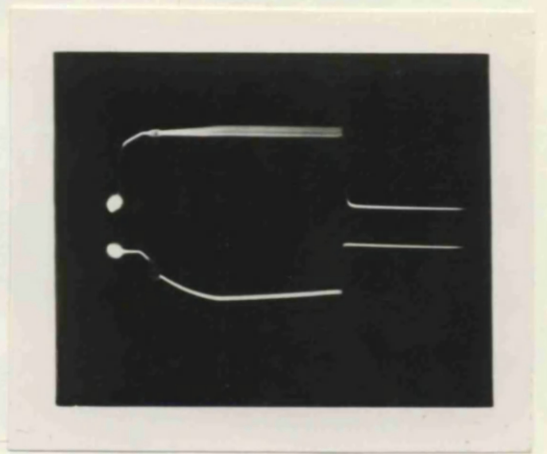
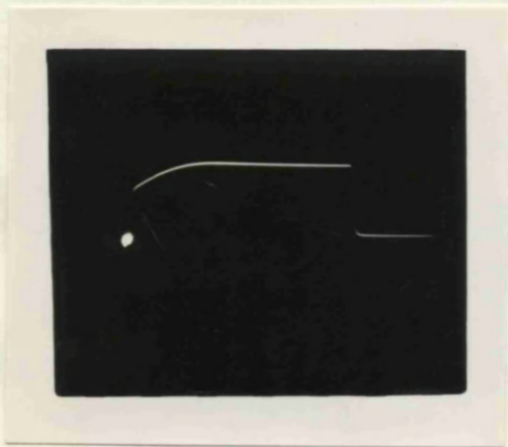


FIG. 46

The modulator pulse was made sensibly square by setting RV1 at minimum value and was displayed simultaneously with the detected RF pulse. These are the upper and lower traces of fig. 46a respectively, in which the pulse width is 6 ms. The apparent drop in amplitude along the detected RF pulse was due to the time-constant of the oscilloscope A2 amplifier.

On introduction of a slow linear rise to the modulator pulse, it was observed that the front edge of the RF envelope was also slowed up, roughly exponentially, but that a delay occurred between the start of the modulator pulse and the beginning of the RF pulse; the length of this delay was dependent on the rate of rise of the modulator pulse.

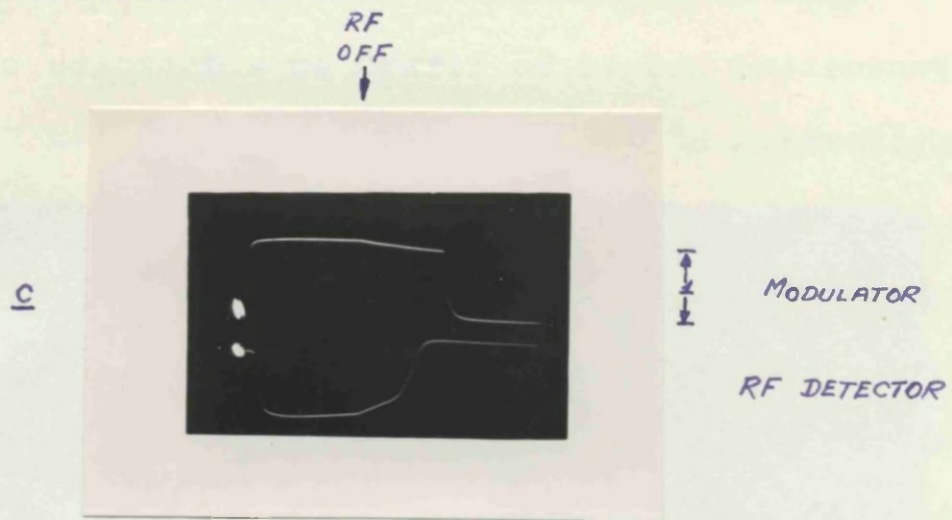
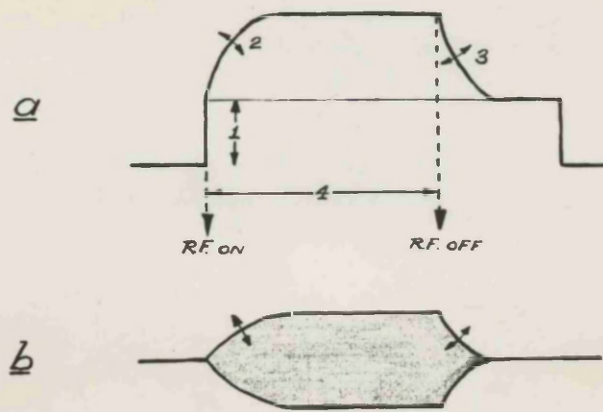
Similar effects were noted with the exponential rise, S open.

This delay indicated that the modulated valve in the transmitter had to be lifted to a definite bias level before application of the slow rise - RV2 catered for this.

Figs. 46b, 46c show the effect of two different exponential rates of rise of the modulator pulse, from which it is seen that the required control of RF build-up can be achieved in this manner. In these traces, the initial step had not been critically adjusted (as it varied in amplitude when the front edge slope was altered) so that a slight delay is still observable between the two pulses. The left hand photograph shows the modulator pulse with the RF off; the upper trace of the right hand photograph is the same pulse with the RF on: it is somewhat affected



FIG. 47



by RF pick-up on the oscilloscope.

On the basis of these results, a new modulator was built to provide a waveform as in fig. 47a, in which the initial pedestal height (1), and the rates of exponential rise and fall of the actual doubler driving portion (2), (3), could be varied independently. When the pedestal height was correctly adjusted to bring the doubler valve to its operating threshold bias, an RF pulse with shaped leading and trailing edges could be obtained, fig. 47b. Fig. 47c shows the modulator and detected RF pulses.

This was tried under operational conditions.

#### 4.3 Experimental Results.

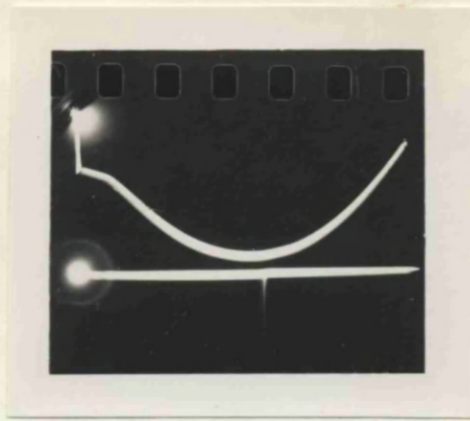
The rise time of the front edge and fall time of the back edge of the modulator pulse could be independently adjusted within the range 50  $\mu$ s - 6 ms; the gap voltages would therefore rise and fall similarly.

A synchrotron beam was built up using the most square edges and the intensity of the X-ray output was observed on the monitor ionization chamber. The electrons lost at transition were observed on the internal probe.

Variation of the rate of rise of the front edge of the RF pulse produced no change in output.

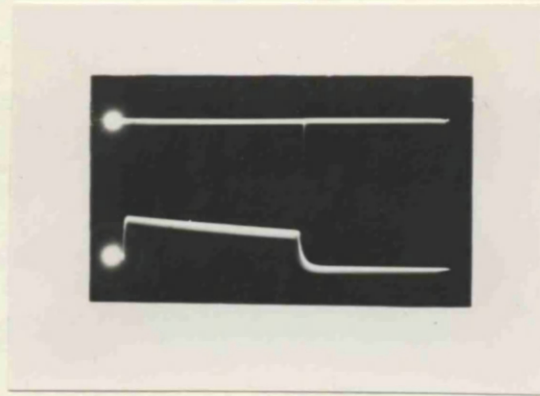
On the other hand, the effect of the back edge shaping was very marked. The RF-off timing was set slightly before peak field with a normal, rapid RF decay and the short X-ray





*FIELD*

*PROBE*



*PROBE*

*RF  
DETECTOR*

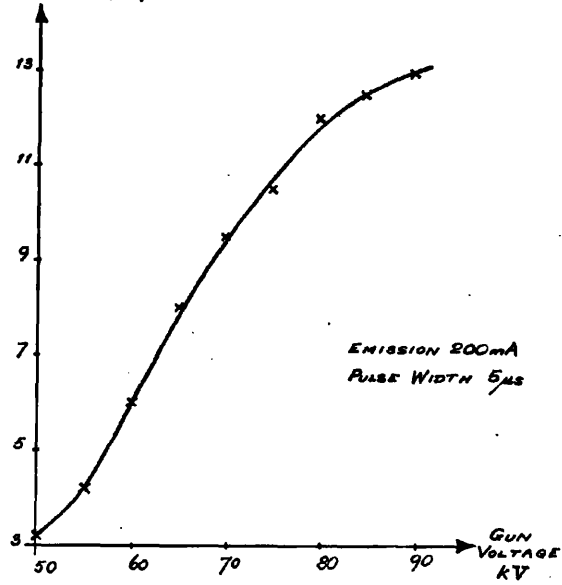
Fig. 48

pulse,  $\sim 50 \mu\text{s}$ , from the internal target was observed on an external 931A detector. The time of fall of the RF pulse was gradually increased while the RF-off timing was simultaneously adjusted to give wide X-ray bursts. The widest pulse observed was  $\sim 3$  milliseconds in length. Fig. 48 shows the short pulse.



RELATIVE  
OUTPUT INTENSITY

FIG. 49



## CHAPTER 5

### MISCELLANEOUS EXPERIMENTS

#### 5.1 Betatron Output Variation with Gun Parameters.

During the period of continuous 50 c/s excitation of the magnet, a number of experiments was carried out on the variation of X-ray output with gun parameters.

The output was observed with an ionization chamber situated in the 15 MeV beam of radiation some three metres from the target.

A steady beam was obtained by adjustment of the magnetic field correction parameters and the gun movements, to give maximum instantaneous reading on the ionization chamber.

With the gun emission set at 200 mA and the gun pulse width at 5  $\mu$ s, the variation of betatron output as a function of gun voltage was observed. The gun voltage was varied from 50 kV to 90 kV in steps of 5 kV and at each setting the injection timing was adjusted to give maximum indicated output.

Above approximately 75 kV, the gun became troublesome and underwent frequent internal breakdown.

Fig. 49 is a plot of the relative output intensity against the gun voltage; this is a smoothly rising curve which indicates that a high gun voltage is desirable.

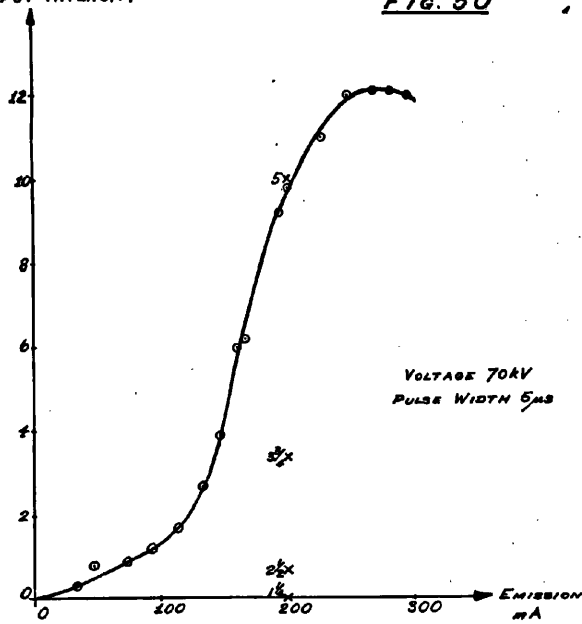
Similar curves were obtained at other values of gun emission.

Following on this work, the gun voltage was set at



RELATIVE  
OUTPUT INTENSITY

FIG. 50



70 kV and the injection timing was adjusted to give maximum steady output at 200 mA emission and 5  $\mu$ s width. Observations were then made on the output variation with gun emission current, this being monitored as the donut coating current (section 3.1).

Fig. 50 is a plot of the results of this experiment and shows that the output intensity rises with increasing gun emission up to a maximum value, which for the particular gun concerned occurred at approximately 300 mA.

Finally with gun voltage at 70 kV, emission at 200 mA, the effect of gun pulse width was observed.

This can be reduced in steps of 1.25  $\mu$ s by removal of sections of the pulse-forming network in the injector modulator, fig. 22.

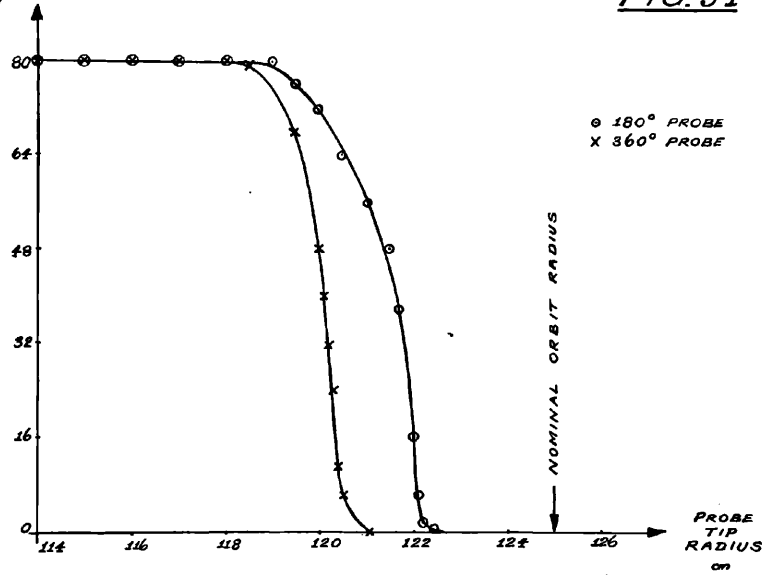
Widths of 5  $\mu$ s, 3.75  $\mu$ s, 2.5  $\mu$ s, 1.25  $\mu$ s were tried; in each case the timing was adjusted for maximum output. The output was found to decrease with shortening of pulse length; the points are plotted in fig. 50 normalized to 10 at 5  $\mu$ s. No estimable output was observed at 1.25  $\mu$ s.

This work indicated the importance of having guns capable of being run for long periods without breakdown, at high voltage and emission, in order to achieve high output intensity.



OUTPUT INTENSITY  
mR/min at 1m

FIG. 51



## 5.2 Aperture Experiments.

Following the work of section 5.1, an investigation was made of the effect on the output intensity of the radial position of the probes.

A steady beam at 70 kV, 200 mA, 5  $\mu$ s was obtained.

Both probes were initially pulled well into their respective ports, then the 180<sup>o</sup> probe was moved into the donut in five millimetre steps. At each position, the intensity indicated by the beam monitor was noted.

The output was at first steady, then fell rapidly and was reduced to nil when the probe tip was approximately 2.5 cm from the nominal orbit radius of 125 cm.

This probe was pulled back into its port and the procedure repeated with the 360<sup>o</sup> probe.

Fig. 51 is a plot of the results.

It will be observed that the 360<sup>o</sup> probe begins to remove electrons from the beam before the 180<sup>o</sup> probe.

This can be explained by considering the oscillatory motion of the electrons following injection. The period of radial oscillation (section 1.3) is given by

$$T_r = T_h (1 - n)^{-\frac{1}{2}} \quad (46)$$

where  $T_h$  is the period of revolution of the electron round the donut.

For  $n = 0.7$ ,  $T_r \doteq 2T_h$ . Thus particles leaving the gun with large oscillation amplitudes viz. the early electrons from the front edge of the gun pulse whose instantaneous circles



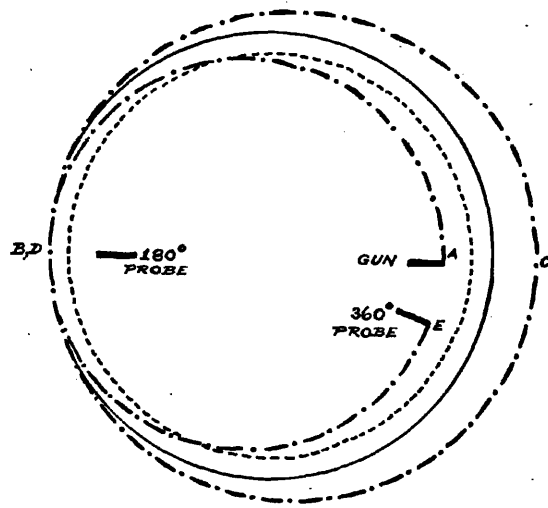


Fig. 52

---

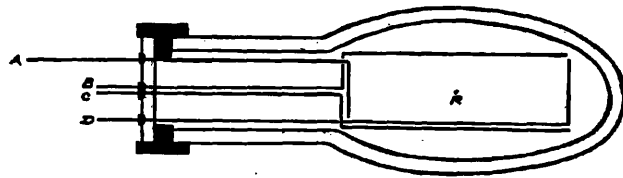


Fig. 53

---

are large, will have little or no deviation from their instantaneous circles halfway round the donut from the gun. In short, the  $180^\circ$  probe is situated near a node of the electron radial motion and the  $360^\circ$  probe near an antinode.

In fig. 52, the dotted circle represents the betatron orbit, the chained curve ABCDE the path of an electron the instantaneous circle of which, at injection, is represented by the full circle.

This particle misses the  $180^\circ$  probe but strikes the  $360^\circ$  probe on its second revolution. Both probes are at the same radius.

In this way the  $360^\circ$  probe affects the beam at smaller radii than the  $180^\circ$  probe.

Later, when the machine was operating as a synchrotron, another aperture limiting device was used. This consisted of a mesh of four tungsten wires A, B, C, D, fig. 53, which passed through O-ring vacuum seals in a perspex plate on the end of a port. The wires were arranged to restrict the donut aperture to a rectangle; A and D were movable radially, one on each side of the nominal orbit R, and B and C were rotatable so that their horizontal portions restricted the vertical aperture. All the wires were earthed to prevent loss of the beam due to their charging up.

The wires were set to give the largest possible rectangle and the effect of each wire separately was observed.

Curves similar to those of fig. 51 showing a rapid fall in intensity were obtained and it was then possible to determine the position of the centre of the electron beam in the donut.

This device was tried at a few points in the donut. As a result it was found that the donut was not situated centrally in the magnet gap at several places and also the orbit was somewhat distorted near the gun.

In addition the experiment showed that the full aperture was used during the synchrotron phase in contrast to the betatron experiment.

## CHAPTER 6

### USE OF THE SYNCHROTRON IN NUCLEAR PHYSICS

#### 6.1 Introduction.

Recent investigations in nuclear physics are concerned with the structure of the atomic nucleus and in this field the high energy synchrotron plays an important role.

By present concepts, the atom is regarded as consisting of a central positively-charged nucleus, which constitutes the major part of the atomic mass, contained within an exceedingly small region of some  $10^{-13}$  cm radius.

Surrounding the nucleus and bound to it by Coulomb electrical forces, is a cloud of tiny negatively-charged electrons, extending to distances of some  $10^{-8}$  cm radius.

The total electron charge balances the nuclear charge to result in a normal, neutral atom.

All the chemical and major optical properties of the atom are due to the planetary electrons.

Nuclei consist of agglomerations of protons and neutrons, which are particles of nearly equal mass. The proton is positively-charged, the neutron neutral.

Chemically different elements have nuclei differing in number of constituent protons; isotopes are chemically indistinguishable nuclei with different numbers of neutrons.

Not all combinations of protons and neutrons are stable, several naturally occurring elements exhibit the

phenomenon of radioactivity whereby the nucleus emits particles or radiation, of energy a few MeV, simultaneously undergoing transformation of species.

Study of the interaction of these emitted radiations with stable nuclei, led to the discovery of artificial radioactivity.

The development of the various particle accelerators provided intense beams of high energy particles for use as projectiles to induce radioactive changes in the nuclei of target atoms. By study of the ensuing reactions and decay processes, considerable data on nuclear transformations and energy levels has been amassed.

In view of the small size of the nucleus, strong binding forces must exist among the constituent nucleons which overcome the mutual Coulomb repulsions between the protons. Since neutrons are uncharged, these forces are not electrical and they are termed nuclear forces. The determination of their exact nature is the central problem of nuclear physics.

Cosmic ray studies led to the discovery of mesons, particles intermediate in size between electrons and protons, sometimes emitted by disrupting nuclei. Their existence had been predicted theoretically by Yukawa 73 in the formulation of a theory of nuclear forces, in which mesons bear to the field of nuclear force the relationship of photons to the extra-nuclear

Coulomb field. On this analogy, a vigorously accelerated nucleon was expected to cause emission of mesons in much the same manner that photons are emitted by accelerated electrons.

Mesons have been produced artificially from target nuclei undergoing bombardment by energetic  $\alpha$ -particles, protons, and by  $\gamma$ -radiation of  $\sim 150$  MeV or more.

The main purpose of constructing high energy synchrotrons is to produce mesons and study their properties in attempt to discover their role in nuclear structure and elicit the nature of nuclear forces.

## 6.2 Production of Mesons.

Cosmic ray studies using nuclear emulsions had established the existence of the positive and negative  $\pi$  and  $\mu$  mesons and the  $\pi - \mu$  decay process.

The  $\pi$ -meson was identified with that predicted by Yukawa.

$\pi$ -mesons were first artificially produced with the 184 in cyclotron at the University of California, and detected by nuclear plates placed near the target which was undergoing bombardment by 380 MeV  $\alpha$ -particles.

The first production by photons also took place at Berkeley 74 using the 335 MeV synchrotron beam.

Later, neutral  $\pi$ -mesons were produced with the synchrotron 75, 76.

The synchrotron has the advantage over the cyclotron

in regard of background radiation, since the beam consists only of bremsstrahlung photons and unconverted electrons - the latter are easily removed magnetically. In the case of the cyclotron, the heavy particle beam gives rise to a background of energetic protons; elaborate arrangements are necessary to discriminate between this and meson producing interactions.

On the other hand, the cyclotron beam is of a definite energy and intensity whereas the photon beam (produced by sensibly monoenergetic electrons striking a target) exhibits the bremsstrahlung, continuous energy spectrum from zero to the peak electron energy, in which the number of photons with energy  $E$  is roughly proportional to  $\frac{1}{E}$ . Thus in general, the energy of a photon responsible for any given event is not known.

The energy spectrum can be ascertained by studying the production of electron pairs in a converter placed in the photon beam, using either a cloud chamber 77, or magnetic pair spectrometer 78.

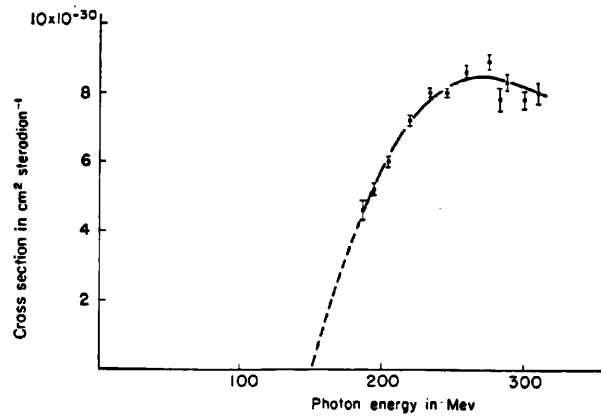
A problem of some difficulty is the calibration of the beam-monitoring ionization chambers in terms of the photon flux 79.

The basic reactions for photo-production of mesons are





Fig. 55



Absolute cross sections for the production of  $\pi$  mesons by the reaction  $\gamma + p \rightarrow n + \pi^-$  as a function of photon energy, according to Bishop, Steinberger, and Cook

If a target of liquid hydrogen is used,  $\pi^+$  and  $\pi^0$  mesons are produced; with carbon or paraffin targets both  $\pi^+$  and  $\pi^-$  types are produced.

Threshold energies for single meson production in colliding systems of elementary particles were evaluated by Barkas 80. Using  $m_\pi = 286m_e$ , the values were:-

$$\gamma + p \rightarrow n + \pi^+ \quad 159 \text{ MeV}$$

$$\gamma + C^{12} \rightarrow B^{12} + \pi^+ \quad 161 \text{ MeV}$$

$$\gamma + C^{12} \rightarrow N^{12} + \pi^- \quad 165 \text{ MeV}$$

Bishop et al 81, using a liquid hydrogen target, measured the photo--meson production as a function of energy and angle of emission and thus calculated the energy of the photon producing the meson. Knowing the number of photons as a function of energy, they then found the meson yield in terms of photon energy. Fig. 55 shows their results; the extrapolated threshold is  $\sim 160$  MeV.

Apart from the use of nuclear plates, delayed coincidence techniques are employed to identify  $\pi$ -mesons in virtue of the  $\pi - \mu$  decay. Neutral mesons are detected by coincident production of two energetic photons, each  $\sim 70$  MeV, the meson decay products.

$$\pi^0 \rightarrow 2\gamma$$

A summary of the properties of mesons is given in reference 82.

## REFERENCES

- 1 Kerst. Phys. Rev. 60 47 (1941)
- 2 Kerst, Serber. Phys. Rev. 60 53 (1941)
- 3 Kerst. Rev. Sci. Inst. 13 387 (1942)
- 4 Bohm, Foldy. Phys. Rev. 70 249 (1946)
- 5 Schiff. Rev. Sci. Inst. 17 6 (1946)
- 6 Iwanenko, Pomeranchuk. Phys. Rev. 65 343 (1944)
- 7 McMillan. Phys. Rev. 68 144 (1945)
- 8 Blewett. Phys. Rev. 69 87 (1946)
- 9 Elder, Langmuir, Pollock. Phys. Rev. 74 52 (1948)
- 10 Schwinger. Phys. Rev. 75 1912 (1949)
- 11 Fremlin, Gooden. Rep. Prog. Phys. 13 295 (1950)
- 12 Livingston. Advances in Electronics 1 269 (1948)
- 13 Crittenden, Parkins. J. A. P. 17 444 (1946)
- 14 Skaggs, Almy, Kerst, Lanzl. Phys. Rev. 70 95 (1946)
- 15 Clark, Getting, Thomas. Phys. Rev. 70 562 (1946)
- 16 Wideroe. Phys. Rev. 71 376 (1947)
- 17 Kerst, Koch. Rev. Sci. Inst. 18 681 (1947)
- 18 Goward, Dain. Nature 159 636 (1947)
- 19 Courant, Bethe. Rev. Sci. Inst. 19 632 (1948)
- 20 Lawson. Nature 166 234 (1950)
- 21 Fawcett, Crittenden. Rev. Sci. Inst. 21 935 (1950)
- 22 De Packh, Haeff. Phys. Rev. 72 247 (1947)
- 23 Adams. Rev. Sci. Inst. 19 607 (1948)
- 24 Kerst. Phys. Rev. 74 503 (1948)
- 25 Heymann. Phys. Rev. 75 1951 (1949)

- 26 Westendorp, Elder. Phys. Rev. 76 445 (1949)
- 27 Jones et al. Phys. Rev. 78 60 (1950)
- 28 Kerst et al. Rev. Sci. Inst. 21 462 (1950)
- 29 Davis. Rev. Sci. Inst. 21 971 (1950)
- 30 Barden. Proc. Phys. Soc. B64 85 (1951)
- 31 Westendorp. J. A. P. 16 657 (1945)
- 32 Kerst. Phys. Rev. 68 233 (1945)
- 33 Amaldi, Ferretti. Rev. Sci. Inst. 17 389 (1946)
- 34 Gregg. Rev. Sci. Inst. 22 176 (1951)
- 35 Wideroe. J. A. P. 22 362 (1951)
- 36 Koch, Robinson. Rev. Sci. Inst. 19 36 (1948)
- 37 Westendorp, Charlton. J. A. P. 16 581 (1945)
- 38 Oliphant, Gooden, Hide. Proc. Phys. Soc. 59 666 (1947)
- 39 Veksler. C. R. Acad. Sci. URSS 43 329 (1944)  
44 365 (1944)
- 40 Veksler. J. Phys. USSR 9 153 (1945)
- 41 McMillan. Phys. Rev. 68 143 (1945)
- 42 Goward, Barnes. Nature 158 413 (1946)
- 43 Frank. Phys. Rev. 70 177 (1946)
- 44 Rabinovich. J. Phys. USSR 10 523, 530 (1946)
- 45 Corben, Stehle. "Classical Mechanics" Art. 72 : Wiley
- 46 Born. "Mechanics of the Atom" : Bell (1927)
- 47 Pollock. Phys. Rev. 69 125 (1946)
- 48 Crane. Phys. Rev. 69 542 (1946)
- 49 Dennison, Berlin. Phys. Rev. 69 542 (1946)  
70 764 (1946)

- 50 Serber. Phys. Rev. 70 434 (1946)
- 51 Blachman, Courant. Rev. Sci. Inst. 20 596 (1949)
- 52 Kaiser, Greanias. Phys. Rev. 69 536 (1946)
- 53 Blewett. J.A.P. 18 968, 976 (1947)
- 54 Gooden et al. Proc. Phys. Soc. 59 677 (1947)
- 55 Twiss, Frank. Rev. Sci. Inst. 20 1 (1949)
- 56 Hibbard. Nucleonics 7 no.4 (1950)
- 57 Courant et al. Phys. Rev. 88 1190 (1952)
- 58 Blake. BTH Report L4014 (1951)
- 59 Goward. Proc. Phys. Soc. A62 617 (1949)
- 60 Wilkins. Phil. Mag. 41 34 (1950)
- 61 Kaiser. Proc. Phys. Soc. A63 52 (1950)
- 62 De Packh, Birnbaum. Rev. Sci. Inst. 21 451 (1950)
- 63 Kaiser. Proc. Phys. Soc. B64 502 (1951)
- 64 Rogers. AERE Report G/R 965 (1952)
- 65 Parzen, Yalow. El. Communication 24 94 (1947)
- 66 Dain, Goward. AERE Reports AE1001, AE1003 also 18
- 67 Williams, Moody. J.I.E.E. 95 IIIA no.7
- 68 Radiation Laboratory Series Vol. 19 : McGraw-Hill
- 69 Curran. "Luminescence and the Scintillation Counter" :  
Butterworth
- 70 Birks. "Scintillation Counters" : Pergamon
- 71 Rodda. "Photoelectric Multipliers" : MacDonalđ
- 72 "Cornell University 300 MeV Synchrotron" July 1953
- 73 Yukawa. Proc. Phys.-Math. Soc. Japan 17 48 (1935)
- 74 McMillan et al. Science 110 579 (1949)
- 75 Steinberger et al. Phys. Rev. 78 802 (1950)

- 76 Panofsky et al. Phys. Rev. 86 180 (1952)
- 77 Powell et al. Phys. Rev. 81 213 (1951)
- 78 Ashkin et al. Phys. Rev. 83 505 (1951)
- 79 Blocker et al. Phys. Rev. 79 419 (1950)
- 80 Barkas. Phys. Rev. 75 1109 (1949)
- 81 Bishop et al. Phys. Rev. 80 291 (1950)
- 82 Thorndike. "Mesons-A Summary of Experimental Facts" :  
McGraw-Hill
- 83 Schwinger. Phys. Rev. 70 798 (1946)